Synthesis and characterization of Beta zeolites for catalytic applications: influence of synthesis parameters

Master of science Thesis

Anna Zaykovskaya

Laboratory of Industrial Chemistry and Reaction Engineering

Faculty of Science and Engineering

Åbo Akademi University

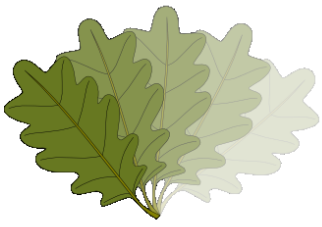

Johan Gadolin

Process Chemistry Centre

Turku/Åbo, 2018

ABSTRACT

Zaykovskaya Anna Olegovna

Synthesis and characterization of Beta zeolites for catalytic applications: influence of synthesis parameters

Master's Thesis

Carried out under the supervision of Prof. Dmitry Yu. Murzin and Docent Narendra Kumar at the Laboratory of Industrial Chemistry and Reaction Engineering, Faculty of Science and Engineering,
Åbo Akademi University

Keywords Zeolites, Beta zeolites, catalytic material, catalyst synthesis, catalyst characterization

The aim of this work is synthesis and physico-chemical characterization of Beta-zeolite catalysts using various synthesis parameters, and their further application in catalytic processes.

Beta-zeolite catalysts were synthesized by two different methods varying such synthesis parameters as time, pH, synthesis temperature, gel composition and gel ripening. Proton forms were obtained by an ion exchange of sodium forms.

Determination of the physico-chemical characteristics of the synthesized catalysts is essential for understanding of catalytic properties of zeolite materials. A range of analytical methods was applied in this work including nitrogen physisorption to analyze surface area, pore volume, and pore size distribution; scanning electron microscopy to study the morphology (shape, size, and distribution of crystals); energy dispersive X-ray spectroscopy for the quantitative study of the elemental composition; transmission electron microscopy to determine the structure and size of pores; temperature-programmed CO_2 desorption to determine the basicity (presence, number and strength of the main areas); temperature-programmed desorption of NH_3 to assess the acidity (presence, amount and strength of acid sites), X-ray powder diffraction to determine the structure, crystallinity and phase purity. Other methods used to characterize the catalysts were nuclear magnetic resonance spectroscopy – ^{27}A1-MAS-NMR and ^{29}Si-MAS-NMR for analyzing the

framework and speciation of A1 and Si in Beta zeolite; Fourier transform infrared spectroscopy to study the acidic properties of the H-Beta-zeolite catalyst for the presence of Brønsted and Lewis acid sites, their number and strength.

PREFACE

The present Master of Science Thesis work was performed at the Laboratory of Industrial Chemistry and Reaction Engineering, (Åbo Akademi University, Turku, Finland) during the period 1.2.2018-30.7.2018.

I would like to express my appreciation to Professor Esther M. Sulman and Professor Valentina G. Matveeva for their support, faith in me, and giving me a chance to be engaged in this Double Master 's program.

I would like to express my deep appreciation to my supervisors – Docent Narendra Kumar and Professor Dmitry Yu. Murzin for their great help with my thesis work and my new knowledge.

Besides, I would like to thank Atte Aho and Kari Eränen for their help during the experimental work.

ABBREVIATION, ACRONYMS AND SYMBOLS

EDX – energy-dispersive X-ray spectroscopy

NMR – nuclear magnetic resonance spectroscopy

TPD – temperature programmed desorption

SDD – silicon drift detector

TPD-NH_3 – temperature programmed desorption of ammonia

XRD –X-ray powder diffraction

FTIR – Fourier-transform infrared spectroscopy

SEM – scanning electron microscopy

TEM – transmission electron microscopy

MOR – mordenite

PHAPTMS – Phenylaminopropyl-trimethoxysilane

GR – gel ripening

R – rotation mode

S – static mode

M1 – 1^{st} method of preparation

M2 – 2^{d} method of preparation

IE – ion exchange

h – hour

g – gram

nm – nanometer

T – temperature

LAS – Lewis acid sites

BAS – Brønsted acid sites

CONTENT

1. Introduction

Zeolite catalysts with varying pore size, structures, acidic properties (Brønsted and Lewis acid sites), ion-exchange and isomorphous substitution of framework alumina have found applications in several industrial processes in oil refinery, production of petrochemicals, synthesis of speciality and fine chemicals, solving environmental-related problems for industrial waste water and exhaust emission control for the motor-driven engines. The reasons for so many industrial catalytic processes are unique properties of microporous zeolites such as a possibility to tailor the crystal size and distributions, uniform channel systems and creation of varying pore sizes in a given zeolite structure. Furthermore, design of pristine parent Beta zeolite catalysts and their proton forms with well-defined structure, crystal size, Brønsted and Lewis acid sites is of immense importance for catalytic applications. Creation of framework Al and Si species with a particular defined co-ordination, formation of hydroxyl groups such as SiOH, AlOH, $Si(OH)_2$ and A1 (OLTL) are challenging tasks, which need in-depth understanding of the silicate solution chemistry, as well as chemistry of aluminates. It should be noted that zeolite synthesis parameters such as synthesis time, temperature, pH and mode of stirring, influence the formation of different aluminate and silicate species during the preparation of zeolite gel mixtures and their subsequent hydrothermal synthesis at elevated temperature. The insertion of A1 species in the framework of Beta zeolite, formation of Brønsted and Lewis acid sites, zeolite crystal formations, their uniformity and distributions can be influenced by varying synthesis time, temperature and pH of the gel solution. Furthermore, sources of silica and alumina, structure directing organic templates and their addition sequence have a potential of influencing the crystal morphology, pore size distributions and crystallinity of the final synthesized Beta zeolite microporous materials. Hence, an in-depth study of these synthesis parameters is necessary for synthesizing Beta zeolite catalysts with a high crystallinity, tuned Brønsted and Lewis acid sites, suitable crystal morphology, the desired physico-chemical and catalytic properties.

As a result of the work twenty-five Beta zeolite samples were synthesized. Physico-chemical and catalytic properties of Beta zeolite catalysts were studied using different characterization methods. It was shown that received zeolites have a surface area higher than reported in the literature. Besides, the number of Brønsted acid sites in some samples was higher compared to H-Beta-25, H-Beta-150 and H-Beta-300.

2. Theory

2.1 Aluminosilicate zeolite type materials

Zeolites are a special group of aluminosilicates, which are highly crystalline, can contain protons, alkali or alkaline earth metals to counterbalance the charge deficit introduced by replacing silicon by aluminum in the framework [1]. There material have numerous applications as catalysts, adsorbents, sensors, separators and ion-exchangers. Catalytic cracking, alkylation, and isomerization can be mentioned as representative catalytic processes in oil refining and chemical industry [2–6]. The industrial interest in zeolites is due to a combination of several favorable properties, including high surface area, good ion-exchange capability, shape-selectivity, tunable Brønsted and Lewis acid sites, high thermal and hydrothermal stability.

Zeolites are made up of micropores with dimensions close to those of many molecules. This feature has endowed them with the remarkable property of shape selectivity, which makes it possible to discriminate among different substrates according to their size [7].

However, the use of zeolite catalysts is hindered in many reactions involving bulky substrates, which cannot enter the zeolite micropores. In this case, the reaction may occur exclusively over the active sites located on the external surface of the zeolite crystals, which value for a conventional micrometer size zeolite is very small (< 10 $m^2 g^{-1}$) [8].

This drawback of zeolites has been circumvented by the development of hierarchical zeolites, which are characterized by the occurrence of a bimodal pore size distribution within the micro/mesopore ranges [9-11]. In these materials, the zeolitic micropore system is complemented by a secondary porosity, with sizes usually in the mesopore range. Depending on the preparation method and the zeolite structure, the contribution of the secondary porosity may vary in a broad range, with values of the mesopore surface area as high as 200 – 300 $m^2 g^{-1}$. Presence of these mesopores facilitates the accessibility of the zeolite inner active sites to bulky substrates. Likewise, it shortens the diffusional pathway length within the zeolite particles and crystals [12]. Hence, this increased accessibility leads to remarkable changes in the catalytic behaviour of the zeolites: enhanced activities [13,14], better dispersion of deposited metal phase [15,16] and lower deactivation rates [17,18].

2.2 Classification and framework composition of synthetic zeolites

The zeolitic framework comprises TO_4 tetrahedron as the basic building unit with the central T-atom being usually Si or Al [1]. Figure 1 illustrates some common ways of constructing the building blocks of zeolites. Figure 1a in particular displays positions of O atoms, which together with T atoms are represented as spheres. Tetrahedral representations (Figure 1b) show TO_4 tetrahedra with common angles and positions of the O atom in a simplified form. The framework representation (Figure 1c) displays the T – T bonds with the T-atom at the vertices.

Figure 1 – Common ways of representing composite building unit formed from eight tetrahedra in a shape of a cube [1].

The composition of zeolites can be expressed by the following empirical formula:

$$M_{2/n} \times Al_2O_3 \times xSiO_2 \times yH_2O$$

Where n – the cation valence, x = 2–200; y – the amount of water.

Polyhedral composite building units can be described using common names. Figure 2 presents some examples of polyhedral composite building units found in the known zeolite framework types.

The most important types of synthetic zeolites for industry are zeolites of type A, F, L X, Y, W, Beta, ZSM-5, MCM-22, and the natural zeolites mordenite, chabazite, erionite and clinoptilolite.

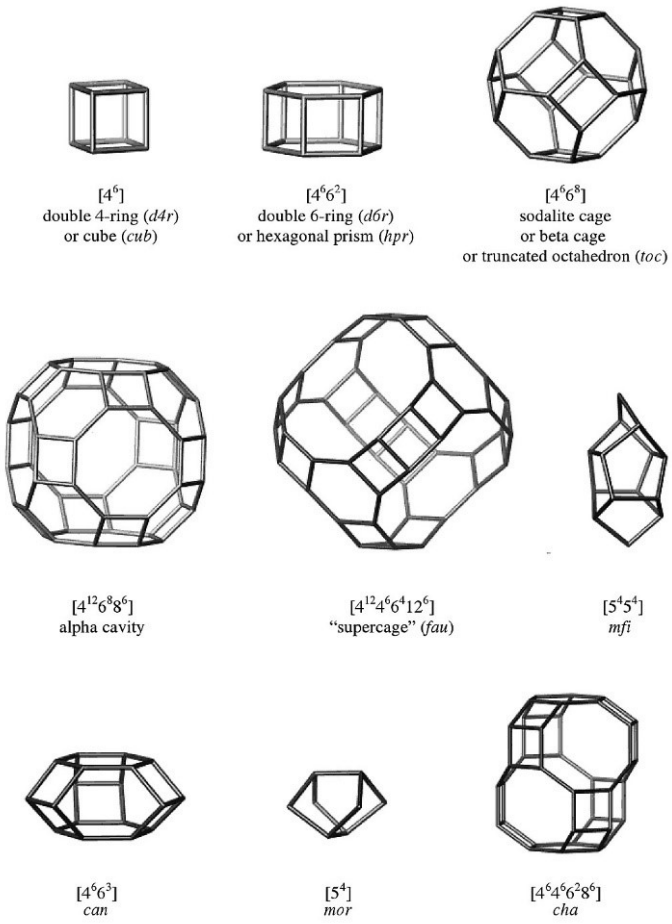

Figure 2 – Polyhedral composite building units and their corresponding common names [1].

In this work zeolites of beta type were studied.

2.3 Beta zeolite

Zeolite Beta has a 3-dimentional structure (Figure 3 a): two 12–membered channels with the pores between 0.76 – 0.64 nm [19]. The unit cell of Beta zeolite structure is tetragonal. Zeolite Beta has been produced industrially for a long time. The laboratory synthetic procedure was created by Camblor and Pérez-Pariente [20].

The gel composition of Beta zeolite can be expressed by the following formula:

$$1.97\ Na_2O : 1.00\ K_2O : 12.5\ (TEA)_2O : Al_2O_3 : 50\ SiO_2 : 750\ H_2O : 2.9\ HCl$$

where TEA is tetraethylammonium hydroxide.

Beta zeolites are often used in fine chemical industries and petroleum refining by reason of its strong acidity and high thermal stability.

The SEM micrograph of Na-Beta-11 and the framework structure of Beta zeolite are presented in Figures 3a and 3b.

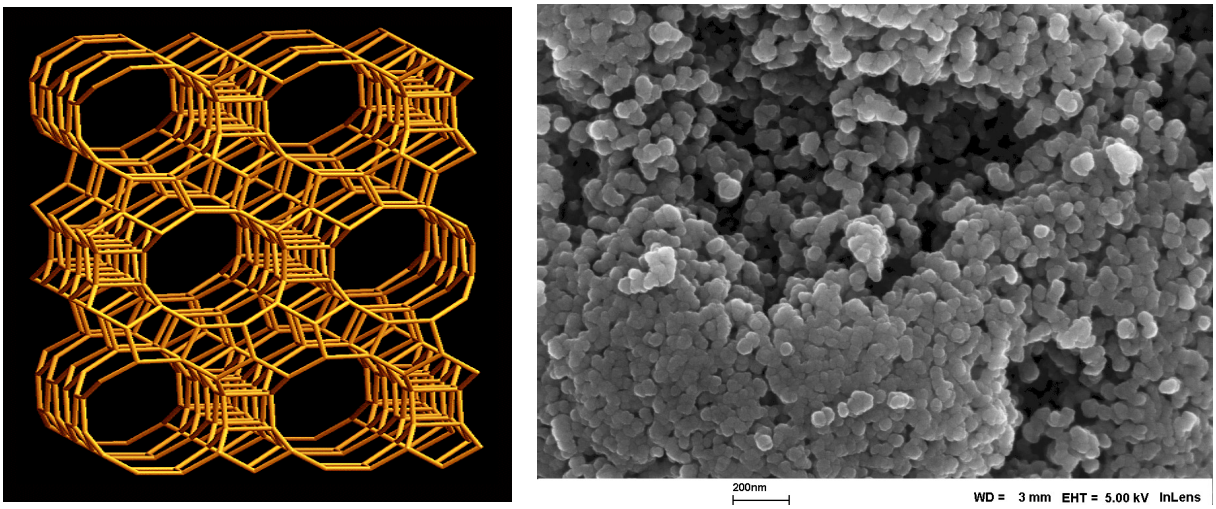

a [20] **b**

Figure 3 – Framework structure of Beta zeolite (a) and SEM micrograph of Na-Beta-11 (b).

2.4 Synthesis of zeolites

Formation of different aluminate and silicate species during the preparation of zeolite gel mixture and its subsequent hydrothermal synthesis at elevated temperature are influenced by such synthesis parameters as temperature, time and pH, as well as the mode of stirring. The insertion of Al species in the framework of Beta zeolite, formation of Brønsted and Lewis acid sites, zeolite crystal formations, its uniformity and distributions can be influenced by varying synthesis time, temperature and pH of the gel solution. Furthermore, sources of silica, alumina, structure directing organic templates and their sequence of addition have the potential of influencing the crystal morphology, pore size distributions, acid sites and crystallinity of the final synthesized Beta zeolites.

Nowadays, efforts are being directed towards developing new types of catalysts based on potentially useful zeolites for various chemical reactions. Numerous research studies have been published.

Zhang et al. [21] demonstrated an approach to synthesizing hierarchical Beta zeolites without usage of any microporous OSDA, PDA, or mesopore templates. This approach combines the advantages of conventional top-down and bottom-up routes for making mesoporous zeolites. The resulting hierarchical Beta zeolites possess large mesopores (10.2 – 14.4 nm) and exhibit considerably improved catalytic activity (product conversion is increased by 35%) as compared to the parent Beta.

Santos et al. [22] studied the effect of the alkaline treatment time at 338 K, varying it from 10 to 240 min for Beta 40 and 73. In the latter case, it was observed that these conditions were too drastic to develop meso-area preserving microporosity: while meso-area was formed easily, only 30% of MiPV was preserved. It seems Beta 40 was a better precursor for following the stepwise transformation during the alkaline treatment. Optimal conditions to create mesopore while maintaining the micropore structure could be found.

First, under mild alkaline treatment, silica is removed from the framework forming mesopores and increasing the area of mesopores. Micropore volume and crystallinity are lost. Some silica is dissolved to the solution and some amorphous phase is formed on the solid (amorphization). The amorphous phase mainly consists of silica.

Then after an increase of the treatment time or performing the treatment under more severe conditions, a part of the amorphous silica returns to the framework in a recrystallization process, diminishing the number of defects. The average size of mesopores is increased and the pore structure is re-organized.

Manrique et al. [23] introduced a new composition in the synthesis gel to prepare zeolite Beta with a low SiO_2/Al_2O_3 ratio ($20<Si/Al<10$ in the final product) at 170ºC in 24 h. The three synthesized zeolites Beta differed significantly in their physico-chemical properties as a consequence of the synthesis conditions variations. The final compositions have shown important effects on the resulting pore system and the acidic properties after calcination. Although the acid strength of solid Brønsted acids is the desired catalytic property for hydrocracking of vacuum gas oil, mesoporosity characteristics should be always taken into account. Acid sites of the moderate strength may exert control over selectivity to gasoline. Moreover, it has been shown that the catalyst formulations with a higher fraction of the zeolite have influenced metal deposition as well as its dispersion. Despite a twofold higher conversion with the catalyst having a higher zeolite content, the middle distillate selectivity was maintained.

Huang et al. [24] reported that one-step and fast synthesis of hierarchical Beta zeolite aggregates, assembled from the nanosized crystals with very small dominant pore sizes, can be successfully achieved by employing H-Kanemite as a layered silicate precursor in hydrothermal conditions using TEAOH as a structure directing agent. Hierarchically structured Beta zeolites with uniform nanosized crystals retain the intracrystal microporosity, and simultaneously possess extremely high mesopore volumes (0.80 - 0.86 mL g^{-1}) and external surface areas (266 - 349 m^2 g^{-1}) derived from the assembly of nanosized crystals. The nanosized Beta zeolite exhibits acidity stronger than the commercial one.

Rutkowska et al. [25] made a comparison of the catalytic performance of different transition metal (Fe, Cu and Co) species introduced to conventional and mesopore-modified Beta

zeolite in N_2O decomposition reaction. The highest N_2O conversion (under conditions simulating the composition of gases emitted from nitric acid plants) was obtained over the Fe-Beta catalyst. This result, together with a high hydrothermal stability (50 h, 773 K), makes this catalyst the most interesting for the application in industry in a studied series of materials.

Jin et al. [26] reported that acidic zeolites with broad Si/Al ratios were modified by alkali–acid treatments, i.e. the sequential combination of alkaline pre-etching, bulk alkaline and acid leaching. H-Beta zeolites that have undergone desilication and dealumination displayed hierarchical porous structures with regular mesopore size distributions, characteristic of pore sizes centering at 4.6-6.1 nm, specific surface areas increasing to 611 m^2 g^{-1} and mesopore volumes up to 0.64 cm^3 g^{-1}. An increase in the framework Al concentration appeared to play a predominant role of controlling desilication, leading to significant mesoporosity with a regular mesopore size distribution. No clear threshold for the initial Si/Al ratio preferable for mesopore modification under the same treatment condition was identified. The combined treatment to Beta zeolites gavr a moderate increase in the Si/Al ratio. Larger losses of the zeolite yields and a relative crystallinity related to excessive dissolution of the parent zeolites.

Besides changes in textural properties of mesopores observed by SEM and TEM, the volumetric fraction of intraparticle to total BJH mesopores decreased from 95.3% to 86.6% as the initial Si/Al ratio increased from 9.4 to 64. Selectivity of T-atoms removal was associated with the Si/Al ratio of the dissolved phases. H-Beta zeolites exhibited selectivity above 95% for desilication and less than 5% for dealumination.

For alkylation of benzene with 1-dodecene, the catalytic performance of hierarchical zeolites Beta was shown to be correlated with the accessible mesoporosity and a regular mesopore size distribution. Both 1-dodecene conversion and linear alkyl benzene selectivity were improved with varying time-on-stream. Despite comparable acidic properties, the modified sample was shown to have a narrow mesopore size distribution and hence to exhibit the enhanced catalytic performance for selective production of linear alkylbenzenes compared with the purely desilicated sample with a broader mesopore size distribution. A correlation between acidity and the hierarchical structure indicated that the synergy between the regular mesopore structure and a relatively mild acidity is the key for the modified Beta zeolites to promote alkylation.

Fang et al. [27] described a novel in situ microwave hydrothermal synthesis technique for the NaA zeolite monolithic adsorbent on a honeycomb ceramic matrix. The synthesis process, the morphology and the adsorption/desorption performance of the monolithic adsorbent were systematically investigated. It was indicated that seeding coating can induce formation of pure NaA zeolite on the ceramic support and prevent NaA crystals from further crystalline

transformation. The optimal synthesis process by the microwave hydrothermal treatment required the microwave time of 45 min and the reaction temperature of 160 ºC.

Khalil and Muraza [28] synthesized pure Mordenite (MOR) zeolite with different gel compositions (i.e. Si/Al 12, 25 and 50). A higher alkalinity of the gel mixture was required to obtain pure MOR with a higher Si/Al ratio under the same conditions. Microwave-assisted hydrothermal synthesis of the seed free mordenite zeolite decreased the crystallization time to 12 h while addition of OSDAs in the gel solution further diminished the time to 6 h at the same conditions. On the contrary, minimum 24 h were needed for the crystallization of pure MOR with OSDA under conventional heating. Aging and crystallization time were optimized to get a pure mordenite phase. Aging time of 6 h gave a higher crystallinity while a further increase in the aging time up to 12 h resulted in an amorphous phase. Spherical and rectangular shaped crystals of the size below 1 mm were obtained at optimized conditions.

García-Muñoz et al. [29] prepared the hierarchical Beta zeolite (h-Beta) from a solution with the following molar composition: Al_2O_3:60 SiO_2:15.5 TEAOH:1000 H_2O [30]. Fumed silica, tetraethylammonium hydroxide, aluminium flakes and distilled water were used as starting reagents. The precursor solution was precrystallized in a Teflon-lined stainless steel autoclave under autogenous pressure at 135 °C for 3 days under static conditions. The obtained solid was mixed with an aqueous solution containing organosilane and TEAOH (13% w/w) (TEAOH/SiO_2 = 0.5). Phenylaminopropyl-trimethoxysilane (PHAPTMS) was employed as a silanization agent [31], being added to the precrystallized solution in a proportion of 8 mol% with respect to the total silica content in the gel. The resulting mixture was kept in a reflux system under stirring (100 rpm) at 90 °C for 6 h. Crystallization was carried out in a stainless steel reactor under autogenous pressure at 135 °C for 7 days under static conditions. The solid products obtained were separated by centrifugation, washed several times with distilled water, dried overnight at 110 °C and calcined in air at 550 °C for 5 h.

After Beta zeolite synthesis, the catalysts were characterized and the characterization data are given in Table 1.

Table 1 – Physico-chemical properties of Beta zeolite.

S_{Bet} (m^2/g)	$S_{mes+ext}$ (m^2/g)	V_w (cm^3/g)	T_{max} (°C)	Acid sites (mmol/g)	Si/Al
599	87	0.303	321	0.443	27

Pashkova et al. [32] proposed, a simple and an eco-friendly method to build up zeolite hollow spheres both without a) the use of soft or hard templates for sphere formation, and b) the addition

of tetra-alkyl ammonium cations for templating the ZSM-5 structure (Figure 5). This significantly simplifies the procedure of the synthesis of hollow spheres of zeolite crystals, eliminates both types of templates usually necessary for bimodal material preparation, and eliminates mainly the step of the hollow sphere templating agent removal. Thus, the procedure for preparation of microporous crystalline hollow spheres does not contain additional steps of template removal compared to the conventionally used syntheses of zeolite hollow spheres. Moreover, hollow spheres of ZSM-5 are formed from crystals with a high framework Al content (Si/Al 14) suitable for catalytic and sorption applications.

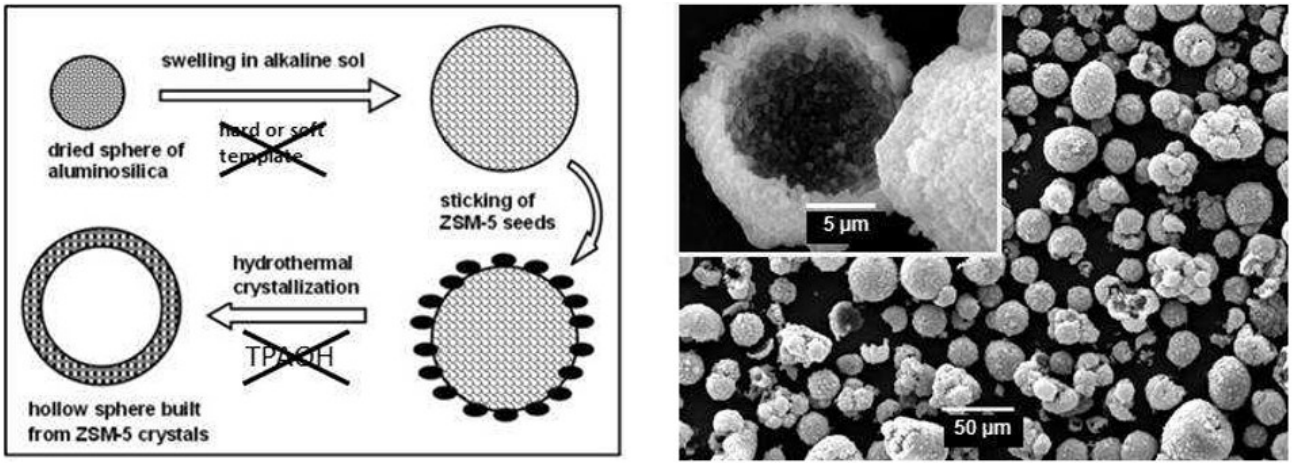

Figure 5 – Self-templating ZSM-5 hollow spheres

The prepared zeolite spheres showed mechanical stability in intensive ultrasonic treatment. Due to a possible stabilization of counter-ion species (H+, metal ions or oxo ions) by the presence of Al atoms in the zeolite hollow sphere network, combined with their shape and high mechanical stability, the prepared materials can be advantageously used in catalytic processes or potentially used for further immobilization of species with a variety of properties. Moreover, due to the fact that the seeding procedure also leads to successful synthesis of other zeolite structures, this approach could be promising for the synthesis of hollow spheres based on various types of industrially important zeolite structures.

Uniform mesopores have been developed [33] in hierarchical Beta zeolite by the application of an ammonia/surfactant hydrothermal treatment. A combination of a mild basic pH with the action of a surfactant provoked a reorganization of the irregular secondary porosity present in the parent zeolite into uniform mesopores with sizes of ca. 40 Å. In contrast, this treatment is less effective when applied to a conventional Beta zeolite sample with a minor secondary porosity.

The main aim of this work is a systematic study of the influence of synthesis parameters such as synthesis time, temperature, pH of the gel mixture, gel ripening and mode of stirring on the physico-chemical and catalytic properties of Beta zeolite catalysts. Beta zeolite synthesis research reported in the open literature is briefly summarized in Table 2.

Table 2 – Comparison of existing methods for the synthesis of Beta zeolites

	Catalyst information						
№	Method of characterization	Material	Si/Al ratio	Surface area ($m^{2}{\cdot}g^{-1}$)	Preparation technique	Calci-nation	Refe-rences
1	XRD, FTIR spectroscopy, TG, DTG and nitrogen adsorption-desorption isotherm analyses	Beta	8	437	hydrothermal method	550 °C for 6 h	[34]
2	PXRD, SEM, HRTEM, TGA and nitrogen adsorption-desorption isotherm analyses	Pure silica	–	455	aging–drying and hydrothermal methods	560 °C for 12 h	[35]
3	XRD, Ar physisorption, NMR, UV/Vis, and FTIR	Sn-BEA-5	20	436	acid dealumination of Beta zeolite, followed by dehydration and impregnation with anhydrous SnCl4	550 °C for 5 h	[36]
4	XRD, ICP-AES, TEM, NLDFT, FTIR, nitrogen adsorption-desorption isotherm analyses	h-Beta	26	727	hydrothermal method		[37]
5		Beta	25	614			
		h-Beta (mnt)	25	520			
		Beta (mnt)	23	540			
6	XRD, FE-SEM, TEM, inductively coupled plasma analysis, HPLC, TG, NH_3-TPD	Meso-Beta	9	660			[38]
		Con-Beta	8.7	629			
		H-Al-Meso-Beta	9.1	643			
7	XRD, nitrogen adsorption-desorption isotherm analyses, elemental analysis, thermal analysis, TPD, FTIR	Beta	25	597	hydrothermal method	550 °C for 2 h	[39]
			50	687			
			70	641			
8	SEM, TEM, DLS, XRD, TG, nitrogen adsorption-desorption isotherm analyses		22	751		600 °C for 2 h	[40]

Continuation of Table 2

	Catalyst information						
№	Method of characterization	Material	Si/Al ratio	Surface area ($m^{2}\cdot g^{-1}$)	Preparation technique	Calci-nation	Refe-rences
9	XRD, TG-DTA, nitrogen adsorption-desorption isotherm analyses		–	443	solvent-free conditions	–	[41]
10	XRD, FTIR, TEM, SEM, ICP, TG, VOCs adsorption, 29Si MAS NMR	Beta-Trans	11	638	synthesized in hydroxide media	600 °C for 6 h	[42]
		Beta-F		525	synthesized in a fluorine ion medium		
		Beta-OH		546	prepared from alkaline media		
		Beta-DA		590	dealumination of Al-Beta zeolite		
11	N_2 Adsorption, XRD, XRF, ICP-OES, NMR	Beta 40	40	716	–	500 °C for 3 h	[22]
12	XRD, FTIR, NMR, SEM, TEM,	T-Beta-20	18	486	hydrothermal method	500 °C for 6 h	[24]

The most suitable method with the highest surface area for synthesis of Beta zeolites was chosen in the current work as a base for future experiments.

3. Experimental

3.1 Synthesis of Beta zeolites

A systematic study of the effect of hydrothermal synthesis parameters was carried out in an autoclave 300 ml (Parr Instruments). The autoclave filled with the gel solution was kept in a temperature-controlled oven. The gel solution was prepared in a 600 ml beaker using various sources of silica, alumina and structure directing templates. After completion of the synthesis, the synthesized material was washed with distilled water, dried in an oven at 110 °C and calcined in a muffle oven.

Two different methods of Beta zeolite preparation were used. According to the first method, 21.0 mL TEAOH (35 wt%, aqueous solution) is mixed with 8.4 mL of water and 4.5 mL HCl (3.7 M). Next, 5.0 g fumed silica is added to the solution under vigorous stirring, followed by a stirring period of 30 min. 0.3812 g $NaAlO_2$ is dissolved in 5.8 mL of water, and subsequently added to the stirring solution. Then, the obtained solution is stirred for one extra hour. Finally, the mixture is divided in two equal parts and transferred into Teflon-lined autoclaves. The autoclaves

are placed in an oven for a hydrothermal treatment in a static mode for different time (24, 48, 72, 96, 120 and 144 h) at 150 °C resulting in the Beta zeolite nanoparticles solutions. After centrifugation and washing with distilled water, drying of the zeolite was performed at 100 °C in an oven. The Beta zeolite was thereafter calcined at 525 °C for 7 h.

In the second method 59.4 g of water, 89.6 g of TEAOH (40%) are mixed with 1.44 g of KCl and 0.53 g of NaCl. Then, 30 g fumed silica is added to the solution and stirred until being homogenized (10 minutes minimum). Next 20.0 g of water is mixed with 0.33 of NaOH and 1.79 g of $NaAlO_2$ and stirred until dissolved. After that, two resulting liquids are combined and stirred for 10 min (gives a thick gel). Finally, the mixture is put in two Teflon cups. The autoclaves are placed in an oven. A subsequent step of centrifugation was followed by washing with distilled water, drying at 100 °C and calcination under static air in a muffle oven at 525 °C using a step calcination procedure. Figure 6 displays the calcination procedure.

For the second method the influence of synthesis parameters such as synthesis time (12, 17, 24 h), temperature (135, 150, 175 °C), pH of the gel mixture (11, 13, 14), gel ripening (2, 4 h) and mode of stirring (static, rotation) on the physico-chemical and catalytic properties of Beta zeolite catalysts was studied.

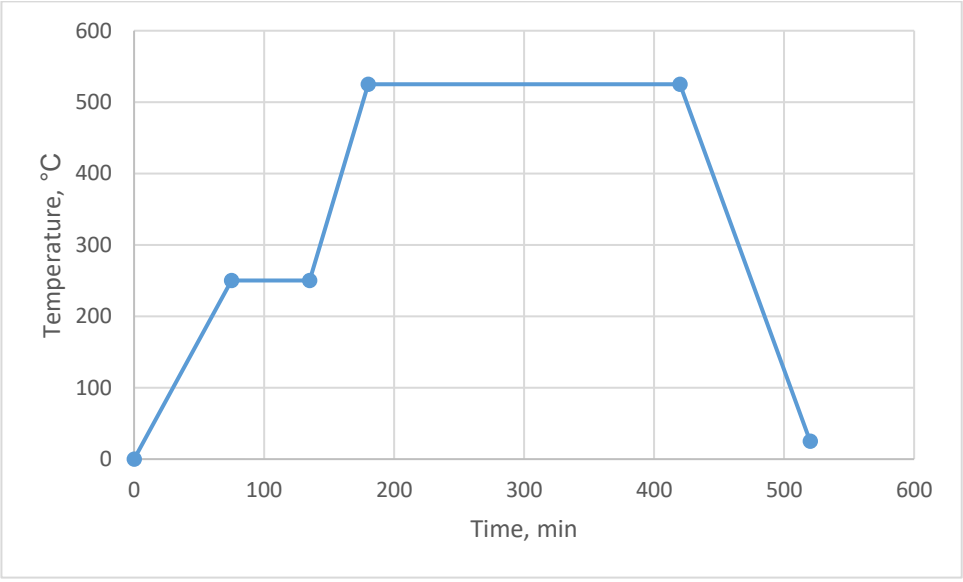

Figure 6 – Step calcination procedure of Na-Beta zeolite synthesized catalysts.

The synthesized Na-form of the Beta zeolite was transformed to H-Beta by an ion-exchange method using an aqueous solution of NH_4NO_3 according to the equation:

$$\text{Na-Beta} + NH_4NO_3 \Rightarrow NH_4\text{-Beta} \Rightarrow \text{H-Beta}$$

Ion exchange was performed using 1 M NH_4NO_3 solution at ambient conditions for 24 hours.

The ion-exchanged zeolite was washed with distilled water until it was free from Cl ions followed by drying at 100 °C. The calcination of NH_4-Beta zeolite for transformation to H-Beta zeolite was performed in a muffle oven using a step calcination procedure (Figure 7).

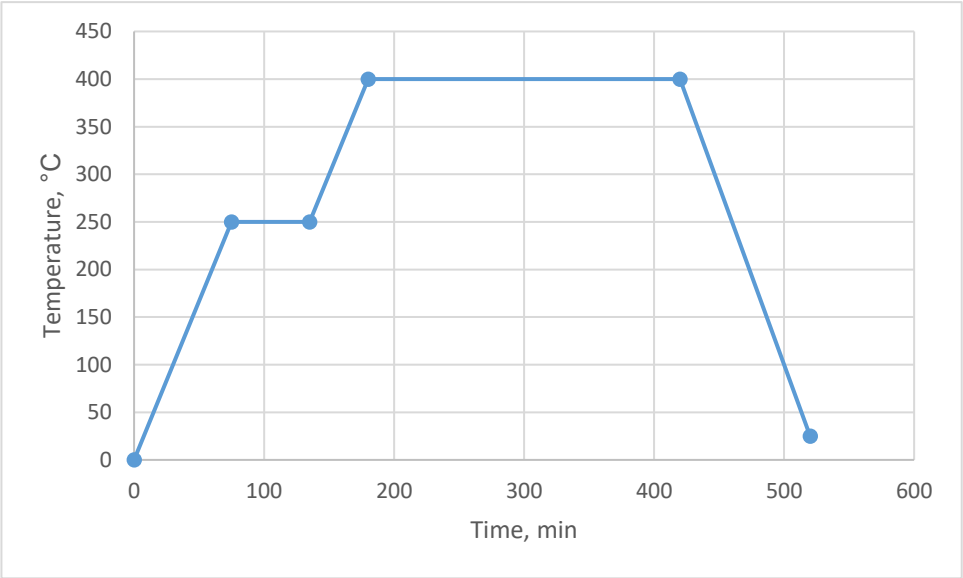

Figure 7 – Step calcination procedure of the NH_4-Beta synthesized catalysts after the ion-exchange process.

3.2 Characterization of prepared materials

3.2.1 N_2-physisorption

Surface area measurements were carried out by nitrogen physisorption using Carlo Erba Instruments (Soptomatic 1900). Calculation of the surface area of the synthesized Beta zeolites was done using the Dubinin method, while the Horvath and Kawazoe method was applied for pore volume calculations.

A typical surface area measurement was performed through the following steps:

1) 0.25 g of catalyst is placed in the previously outgassed burette with a known weight.
2) The catalyst was outgassed in the burette at 423 K for three hours.
3) The outgassed burette with the catalyst was connected to the equipment and placed in liquid nitrogen.

3.2.2 Scanning electron microscopy and energy dispersive X-ray micro-analysis spectroscopy

In the current work, SEM was used to analyze the morphology, distribution of crystals, size and shape of Beta zeolites. The main advantage of SEM is the possibility to observe solid-state topography with a resolution and depth of field far exceeding the corresponding parameters of optical microscopes.

Measurements were carried out using LEO Gemini 1530 with a Thermo Scientific UltraDry Silicon Drift Detector equipped with a secondary electron, a backscattered electron and an In-Lens detector.

Determining of the elemental composition was done using Energy dispersive X-ray micro-analysis spectroscopy (EDX).

3.2.3 Transmission electron microscopy

The morphology, structure, porosity and channel systems of catalysts was investigated with transmission electron microscopy. The measurements were carried out at the Laboratory of Electron Microscopy, Institute of Biomedicine, Faculty of Medicine, Turku University, with a JEM 1400 plus instrument having an acceleration voltage of 120 kV and a resolution of 0.98 nm using a Quemsa II MPix bottom mounted digital camera.

3.2.4 X-ray powder diffraction

The PANalytical Empyrean X-ray powder diffractometer was used for determination of the structural properties and phase purity of Beta zeolite catalysts. The diffractometer was operated in the Bragg-Brentano diffraction mode, and the monochromatized Cu-Kα radiation (λ = 1.541874 Å) was generated with a voltage of 45 kV and a current of 40 mA. The primary X-ray beam was collimated with a fixed 0.25° divergence slit, a fixed 10 mm mask and a fixed 1° anti-scatter slit. A 7.5 mm anti-scatter slit was used in the diffracted beam side prior to the proportional counter. The measured 2θ angle range was 2.0°−80.0°, with a step size of 0.026° and a measurement time of 80 s per step. The samples were ground gently before the measurements to minimize the sample texture (preferred crystal orientation).

The samples were measured on stainless steel sample holders. It must be stressed that the phase detection threshold of this kind of an X-ray powder diffraction measurement is limited to approximately 5%. The measured diffractograms were analyzed with Philips XPert HighScore and MAUD programs. HighScore together with MAUD was used for the phase analysis, while MAUD was utilized for the Rietveld refinement. The Powder Diffraction database, IZA Structure Commission Database of Zeolite Structures and Inorganic Crystal Structure Database (ICSD) were used as sources of reference [43-45]. The crystal structure reference and the corresponding crystal information of Beta polymorph A (Figure 8) (SiO_2 framework) were taken from the IZA Structure Commission Database of Zeolite Structures [46].

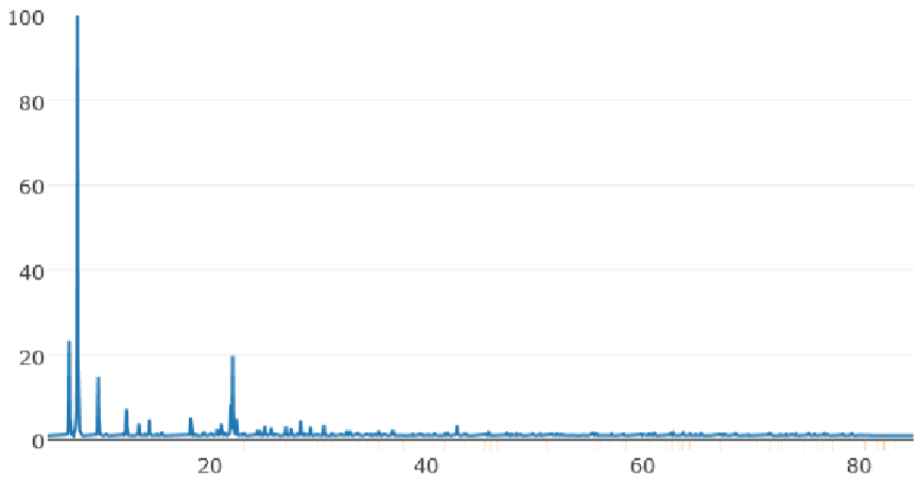

Figure 8 – Typical diffractogram of Beta zeolite polymorph A

3.2.5 ^{27}A1-MAS NMR and ^{29}Si MAS NMR spectrometers

Formation of Brønsted and Lewis acid sites in zeolites is influenced by the location of A1 species in the framework (tetrahedra) and extra framework (octahedra). Identification and analysis of the A1 and Si species in Beta zeolites were carried out using ^{27}A1-MAS NMR and ^{29}Si MAS NMR spectrometers at the Institute of Chemical Physics and Biophysics, Tallinn, Estonia. The results obtained from the analysis were correlated with Brønsted and Lewis acid sites measurements by FTIR using pyridine as a probe molecule.

^{29}Si MAS NMR spectra were recorded on a Bruker AVANCE-II spectrometer in an 8.5 T magnetic field using a home-built MAS probe for 10 mm od zirconia rotors. Single pulse spectra were accumulated with 6 μs pulse (3/8 π) excitation at 71.43 MHz with a repetition time of 100 s at 5 kHz sample spinning speed. The chemical shifts are given in TMS scale.

^{27}Al MAS-NMR spectra were recorded at 208.49 MHz on a Bruker AVANCE-III spectrometer at an 18.8 T external field using a Bruker MAS probe and 3.2 mm zirconia rotors. The spectra were collected by single 0.6 μs pulse (π/18) excitation with repetition time 60ms and 22 kHz sample spinning frequency. The spectra are referenced to the frequency of $Al(NO_3)_3$ solution.

The intensity in the NMR spectra is normalized to the number of accumulations and to the mass of the sample.

3.2.6 Fourier-transform infrared spectroscopy

Acidity of the catalysts was determined with ATI Mattson FTIR of adsorbed pyridine (Sigma-Aldrich, >99.5%, a.r.) as a probe molecule. Infrared transmission spectra were recorded on the thin pressed tablets of ca. 10-20 mg. Pretreatment of the pellets was made at 450 °C for 1 hour at 7 Pa before the measurement. First pyridine was adsorbed for 30 min at 100 °C. To obtain the distribution of weak, medium and strong Brønsted and Lewis acid sites, desorption of pyridine was made at different temperatures: 250, 350 and 450 °C. Brønsted and Lewis acid site concentrations were calculated by the integration of the infrared bands at 1545 cm^{-1} (with 1.67 cm/mm as the molar absorption coefficient) and at 1455 cm^{-1} (with 2.22 cm/mm the molar absorption coefficient), respectively. The molar extinction coefficients were taken from the work of Emeis [47].

4. Results and discussion

4.1. Beta zeolite synthesis results

As a result of the experimental work, 25 Beta zeolite samples were synthesized (Table 3). Beta zeolite catalysts were synthesized by systematic variation of synthesis parameters such as time, temperature, pH of the gel mixture, gel ripening and mode of stirring. Microporous catalysts having a Beta zeolite structure with different physico-chemical and catalytic properties were obtained. All Beta zeolite catalysts were characterized with nitrogen physisorption, X-ray powder diffraction and FTIR using pyridine as a probe molecule. Selected catalysts with promising catalytic application results were further characterized with scanning electron microscopy, ^{27}A1-MAS-NMR and ^{29}Si-MAS-NMR, energy dispersive X-ray micro-analysis and inductively coupled plasma spectrometry.

A data base of the physico-chemical catalyst characterization results was created. This data base could be applied for explanation and correlation of catalytic activity and selectivity with the catalyst structure. Furthermore, catalyst characterization results were utilized for a further development of the Beta zeolite catalysts. Taking into consideration the importance of the zeolite crystal size, shape and distributions in catalytic reactions, special emphasis was put on the tailor-made design of the Beta zeolite crystal size, shape and distribution of crystals. Hence, crystal engineering was an integral part of the research project. It is well known that the presence, amount and strength of Brønsted and Lewis acid sites influence conversion, selectivity to the desired products and product distribution.

Table 3 – Beta zeolite synthesis results

Catalyst	Synthesis conditions	
Na-Beta-M_1	12 h	150 °C- static mode
	24 h	
	144 h	
Na-Beta-M_2	12 h	135 °C-static mode
	17 h	
	24 h	

Continuation of Table 3

Catalyst	Synthesis conditions	
	12 h	135 °C-rotation mode
	17 h	
	24 h	
	12 h	150 °C-static mode
	17 h	
	24 h	
	12 h	150 °C-rotation mode
	17 h	
	24 h	
	17 h	150 °C-rotation mode-(gel ripening-2h)
		150 °C-rotation mode-(gel ripening-4h)
		150 °C-rotation mode, (pH of gel=11)
		150 °C-rotation mode, (pH of gel=14)
Na-Beta-M_2	12 h	175 °C-static mode
	17 h	
	24 h	
	12 h	175 °C-rotation mode
	17 h	
	24 h	

4.2 Beta zeolite physico-chemical characterization results

The survey of physico-chemical characterization results of Beta zeolite is given in Table 4

Table 4 – Survey of Beta zeolite physico-characterization results

	Synthesis conditions		N_2-physis	SEM-EDXA	TEM	XRD	NMR	FTIR
Na-Beta-M_1	12 h	150°C - static mode	+	+	+	+	-	-
	24 h		+	+	+	+	-	-
	144 h		+	+	+	+	-	-
Na-Beta-M_2	12 h	135°C -static mode	+	+	-	-	-	-
	17 h		+	+	-	-	-	-
	24 h		+	+	-	-	-	-

Continuation of Table 4

	Synthesis conditions		N_2-physis	SEM-EDXA	TEM	XRD	NMR	FTIR
	12 h	135 °C-rotation mode	+	+	+	+	-	-
	17 h		+	+	+	+	-	-
	24 h		+	+	+	+	-	-
	12 h	150 °C-static mode	+	+	+	-	+	-
	17 h		+	+	+	-	+	-
	24 h		+	+	+	-	+	-
	12 h	150 °C-rotation mode	+	+	+	+	+	-
	17 h		+	+	+	+	+	+
	24 h		+	+	+	+	+	-
	17 h	150 °C-rotation mode-(gel ripening-2h)	+	+	+	+	-	-
		150 °C-rotation mode-(gel ripening-4h)	+	+	+	+	-	-
		150 °C-rotation mode, (pH of gel=11)	+	+	-	-	-	-
		150 °C-rotation mode, (pH of gel=14)	+	+	-	-	-	-
Na-Beta-M_2	12 h	175 °C-static mode	+	+	-	-	-	-
	17 h		+	+	-	-	-	-
	24 h		+	+	-	-	-	-
	12 h	175 °C-rotation mode	+	+	+	+	-	-
	17 h		+	+	+	+	-	-
	24 h		+	+	+	+	-	-

4.2.1 N_2-physisorption

Surface area measurements were carried out for Beta zeolites by nitrogen physisorption using the Dubinin method for calculation of the surface area and the Horvath and Kawasaki method for

determination of the pore volume. The results of the surface area and micropore volume measurements are shown in Table 5.

Table 5 – Specific surface area

Catalyst	Synthesis conditions		Surface area, m^2/g	Pore volume, cm^3/g
Na-Beta-M_1	12 h	150 °C static	486	0.17
	24 h		501	0.18
	144 h		716	0.25
Na-Beta-M_2	12 h	135 °C static	102	0.04
	17 h		198	0.07
	24 h		677	0.24
	12 h	135 °C rotation	171	0.06
	17 h		659	0.23
	24 h		658	0.23
	12 h	150 °C static	178	0.06
	17 h		708	0.25
	24 h		398	0.14
	12 h	150 °C rotation	442	0.16
	17 h		752	0.26
	24 h		703	0.25
	12 h	175 °C static	675	0.24
	17 h		535	0.19
	24 h		500	0.18
	12 h	175 °C rotation	701	0.25
	17 h		689	0.24
	24 h		556	0.20
	17 h	150 °C rotation, 2h gel ripening	704	0.25
		150 °C rotation, 4h gel ripening	762	0.27

The highest surface area and the micropore volume were achieved using synthesis at 150 °C in the rotation mode for 17 h (752 m^2/g, 0.26 cm^3/g). Then the selected catalyst was subjected to the gel ripening procedure. Four hours of gel ripening increased the micropore volume and the surface area to 0.27 cm^3/g and 762 m^2/g, respectively. An explanation for the increase in the surface area and pore volume for the Beta zeolite synthesized at 150 °C, 17 h (752 m^2/g) and exposed to the gel ripening (762 m^2/g) procedure is the enhanced micro-porosity of the Beta

zeolite. It is noteworthy to mention here, that the surface area of Beta zeolite synthesized in 12 h, 135 °C static), 12 h, 135 °C (rotation), 12 h, 150 °C (static) showed the lowest surface area of 102 m^2/g, 171 m^2/g, 178 m^2/g, respectively. The presence of an amorphous phase, a decrease in the pore dimensions and diminished porosity are the most plausible reasons for such decrease in the surface area.

4.2.2 Scanning electron microscopy

Micrographs of different Beta zeolite materials are shown in this section using 200 nm scale and 25000 magnification.

4.2.2.1 SEM results for the first method of zeolite preparation

Figure 9-11 show SEM results for the first method of zeolite preparation. The samples were prepared using three different synthesis time – 12h, 24h and 144h.

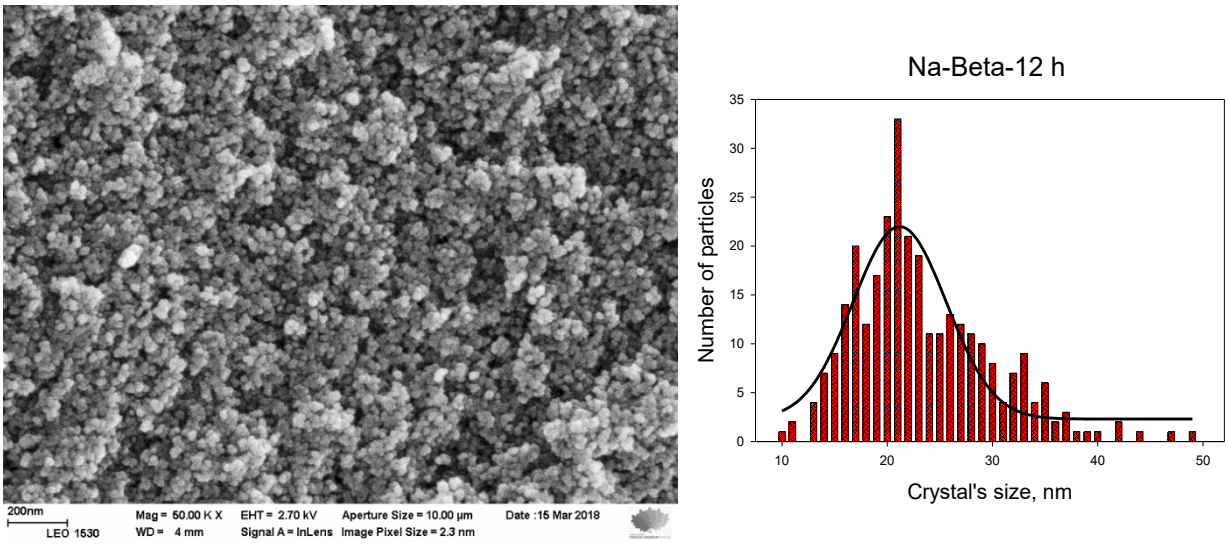

Figure 9 – Scanning Electron Micrograph of Na-Beta-12h-150 °C-static-M_1.

Predominant crystal size: 21 nm.

Average particle size: 23 nm.

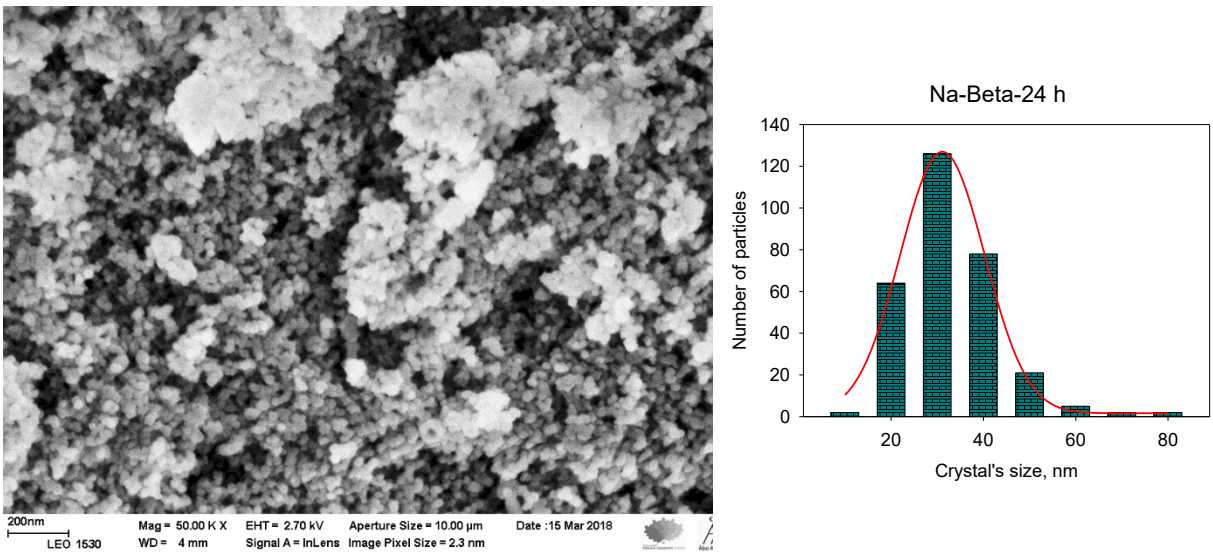

Figure 10 – Scanning Electron Micrograph of Na-Beta-24h-150 °C-static-M_1.

Predominant crystal size: 30 nm.

Aaverage particle size: 38 nm.

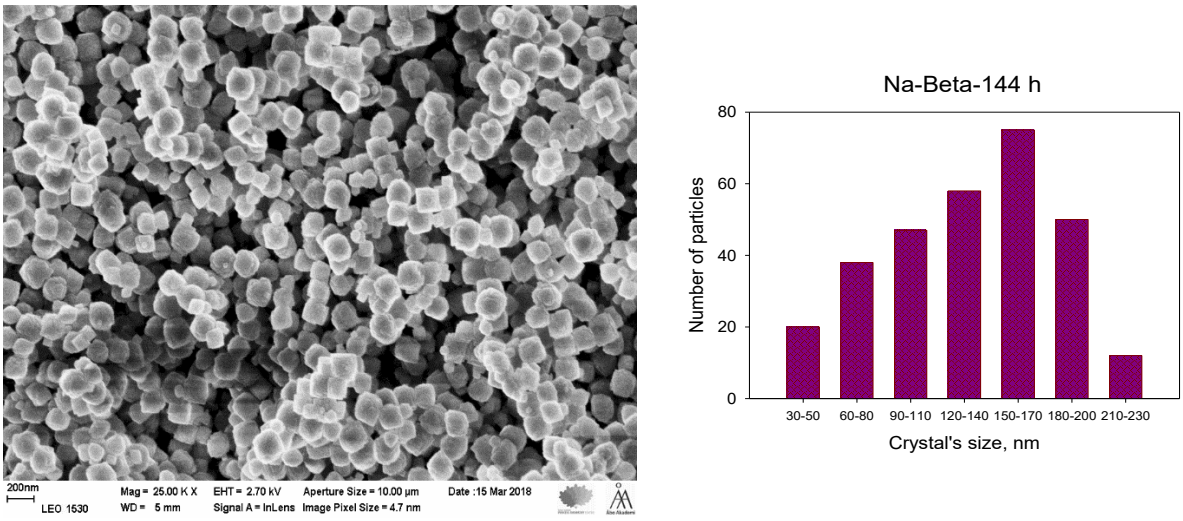

Figure 11 – Scanning Electron Micrograph of Na-Beta-144h-150 °C-static-M_1.

Predominant crystal size: 170 nm.

Average particle size: 138 nm.

It can be seen from Figures 9-11 that an increase of the reaction time (from 12 h to 144 h) influences the crystal structure and size. After 144 h formation of clearly defined round shape crystals of Beta zeolite phase took place. An average crystal size increases with the increasing synthesis time as follows: 23 nm (12 h) > 38 nm (24 h) > 138 nm (144 h), Figure 9-11. The largest average crystallite size was obtained for the Beta zeolite synthesized in 144 h. The Beta zeolite

synthesized in 12 h did not exhibit the typical crystal shape of Beta zeolite, which was confirmed by the X-ray powder diffraction patterns. These patterns for the sample synthesized in 12 h exhibited an amorphous hump typical for the non-crystalline amorphous materials.

4.2.2.2 SEM results for the second method of zeolite preparation

The results of SEM analysis for the second method of zeolite preparation at 135 °C are presented in Figures 12-17.

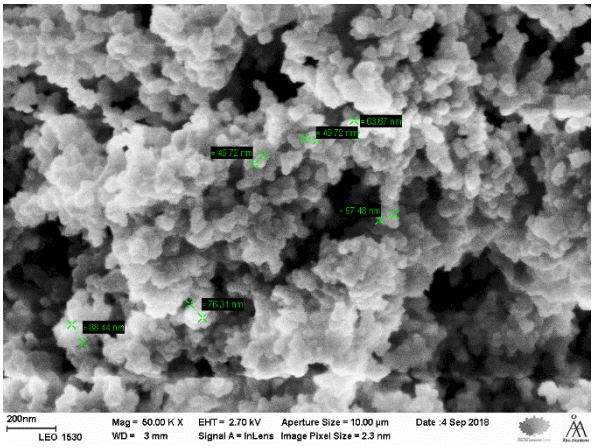

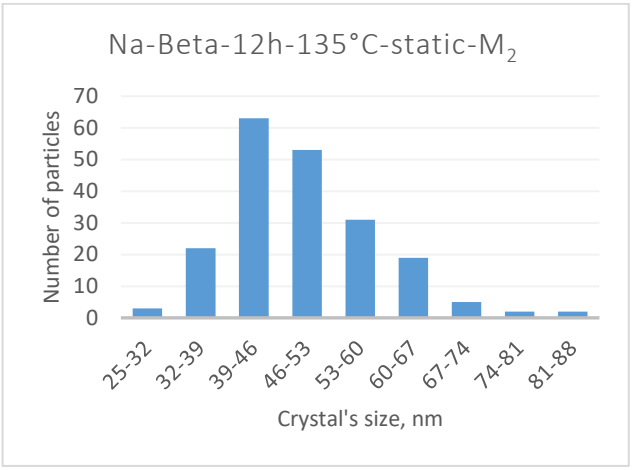

Figure 12 – Scanning Electron Micrograph of Na-Beta-12h-135 °C-static-M_2.

Predominant crystal size: 43 nm

Average particle size: 49 nm

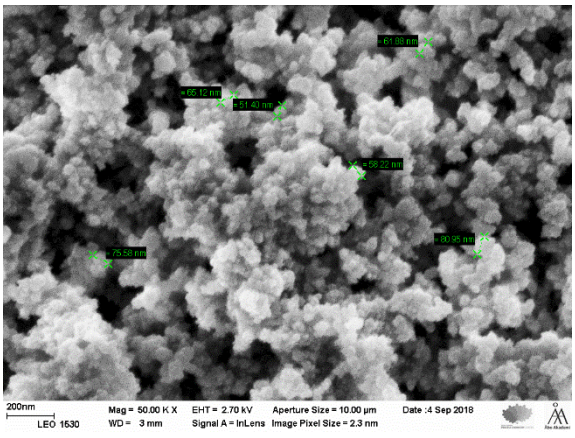

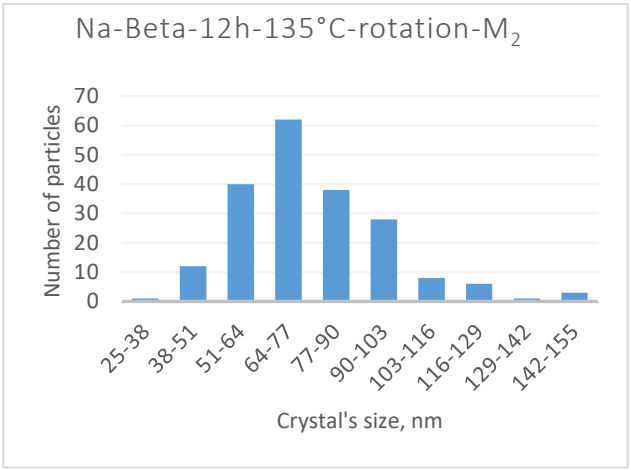

Figure 13 – Scanning Electron Micrograph of Na-Beta-12h-135 °C-rotation-M_2.

Predominant crystal size: 71 nm.

Average particle size: 77 nm.

The Beta zeolite synthesis carried out at 135 °C, 12 h, rotation mode exhibited a larger average crystal size (77 nm) than the average crystal size (49 nm) for the synthesis performed at 135 °C, 12 h, static mode, Figure 12-13. It was inferred from the above result that the rotation mode enhanced the crystal size formation.

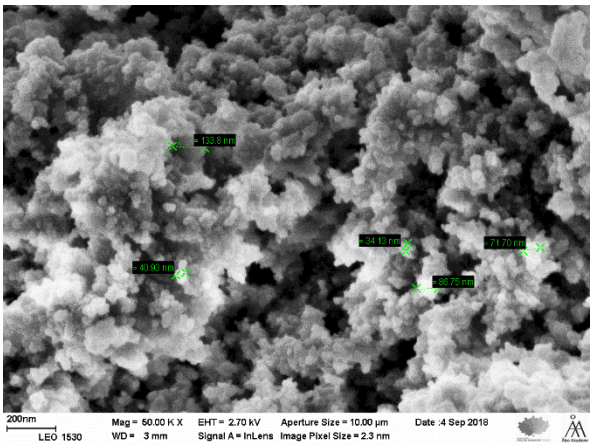

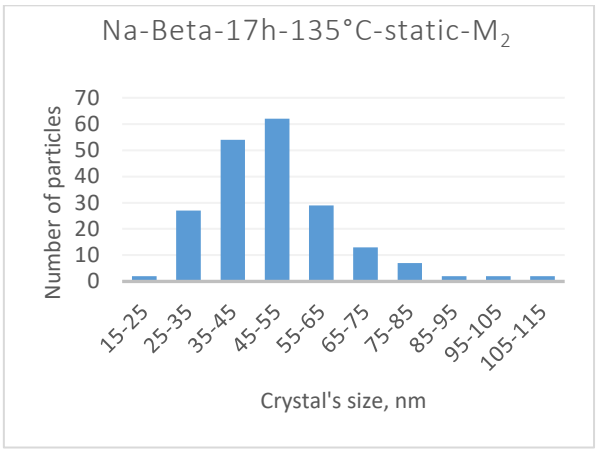

Figure 14 – Scanning Electron Micrograph of Na-Beta-17h-135 °C-static-M_2

Predominant crystal size: 50 nm.

Average particle size: 49 nm.

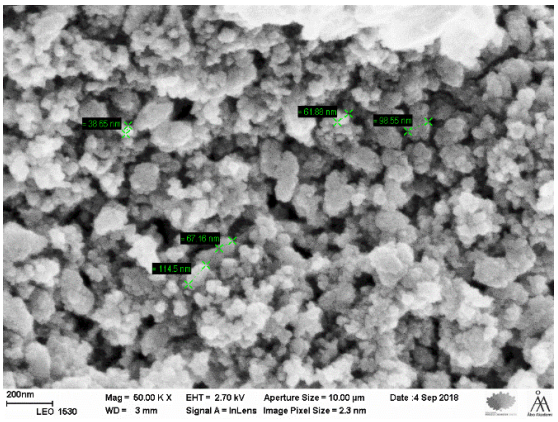

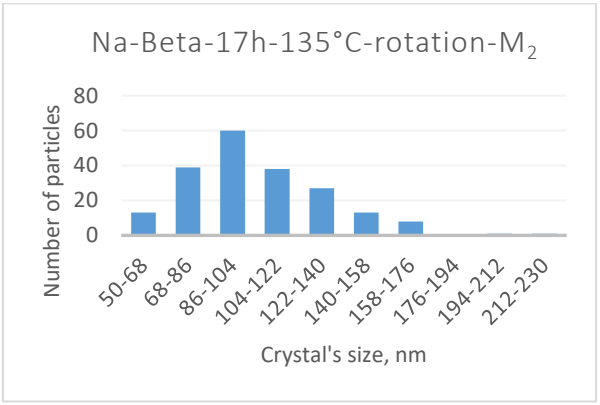

Figure 15 – Scanning Electron Micrograph of Na-Beta-17h-135 °C-rotation-M_2.

Predominant crystal size: 95 nm.

Average particle size: 105 nm.

The Beta zeolite synthesis carried out at 135 °C, 17 h, in the rotation mode also showed an enhancement in the average crystal size (105 nm) compared to the average crystal size (49 nm) synthesized at 135 °C, 17 h, in the static mode, Figures 14, 15.

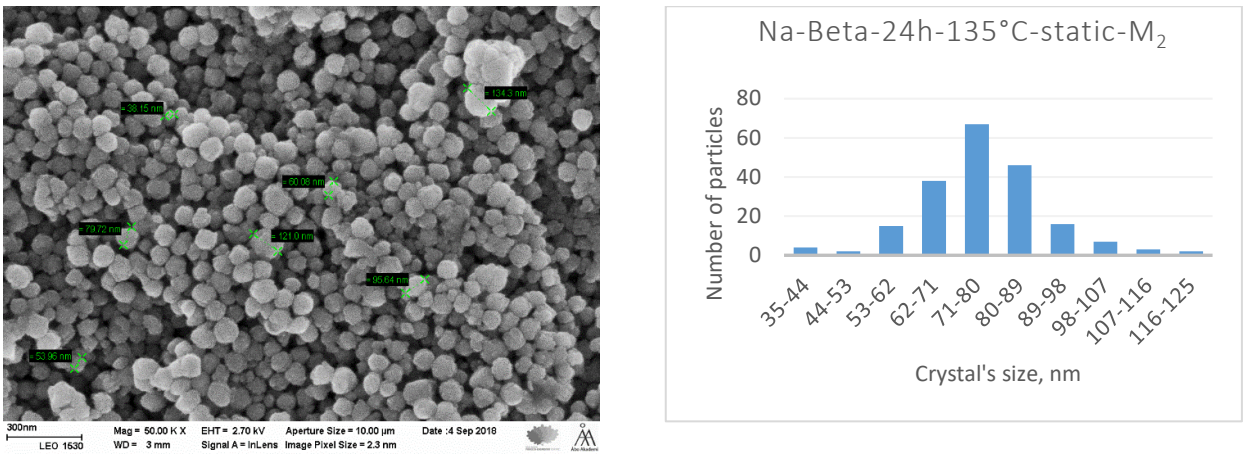

Figure 16 – Scanning Electron Micrograph of Na-Beta-24h-135 °C-static-M_2.

Predominant crystal size: 76 nm.

Average particle size: 77 nm.

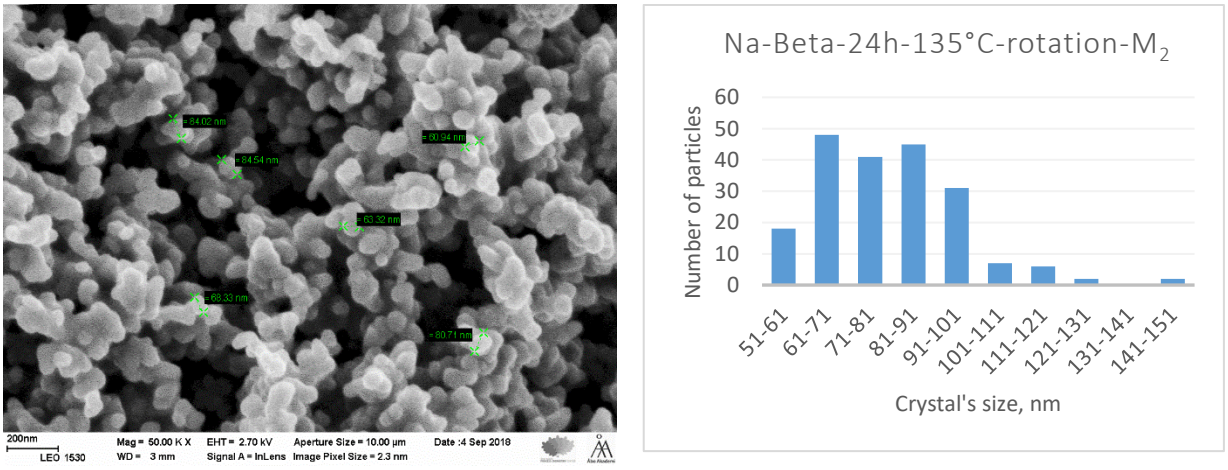

Figure 17 – Scanning Electron Micrograph of Na-Beta-24h-135 °C-rotation-M_2.

Predominant crystal size: 76 nm.

Average particle size: 81 nm.

A similar enhancement in the average crystal size (81 nm) was observed for the synthesis performed at 135 °C in rotation mode for 24 h in comparison with the average crystal size at 77 nm for synthesis carried out in the static mode at 135 °C for 24 h, Figures 16-17. It was inferred that Beta synthesis carried out with an increase in time (i.e. 12, 17, 24 h) with rotation mode exhibited larger average crystal sizes than the static mode.

Most of the catalysts were in the amorphous phase or almost amorphous except for the samples prepared within 24 hours. The reason for the presence of the amorphous phase was a low temperature of 135 °C is too low for the Beta zeolite synthesis. The presence of an amorphous phase was also confirmed by the X-ray powder diffraction characterization.

In Figures 18-25 scanning electron micrographs of Na-Beta samples synthesized at 150 °C are illustrated.

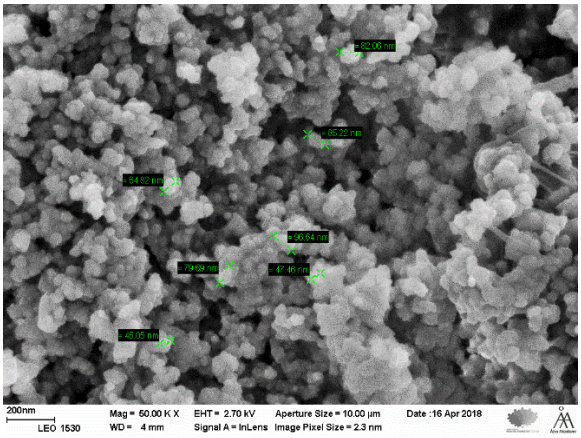

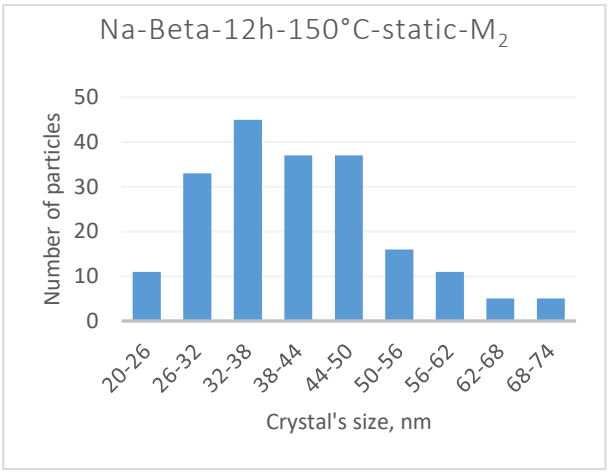

Figure 18 – Scanning Electron Micrograph of Na-Beta-12h-150°C-static-M_2.

Predominant crystal size: 35 nm.

Average particle size: 41 nm.

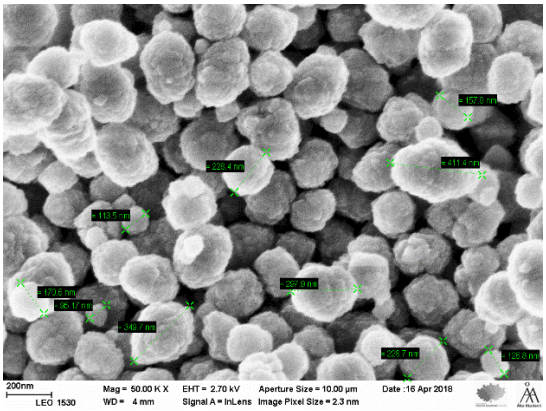

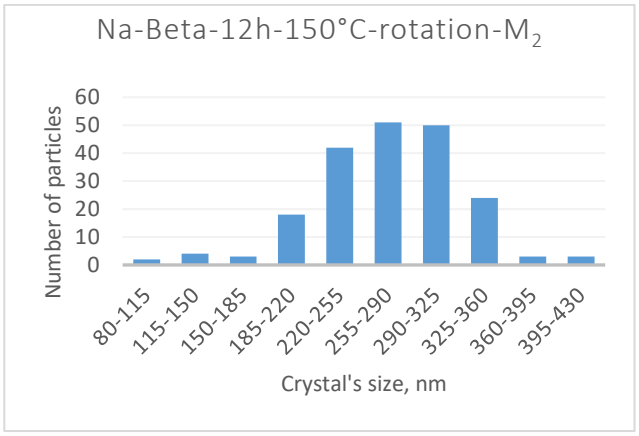

Figure 19 – Scanning Electron Micrograph of Na-Beta-12h-150°C-rotation-M_2.

Predominant crystal size: 290 nm.

Average particle size: 273 nm.

It is noteworthy to mention that after an increase of the temperature to 150 °C for the synthesis at 12 h in the rotation mode larger average crystals (273 nm) were obtained in comparison to the static mode at the same conditions (41 nm), Figures 18, 19. Furthermore, X-ray powder diffraction patterns also confirmed the presence of the crystalline phase and the structure of Beta zeolite.

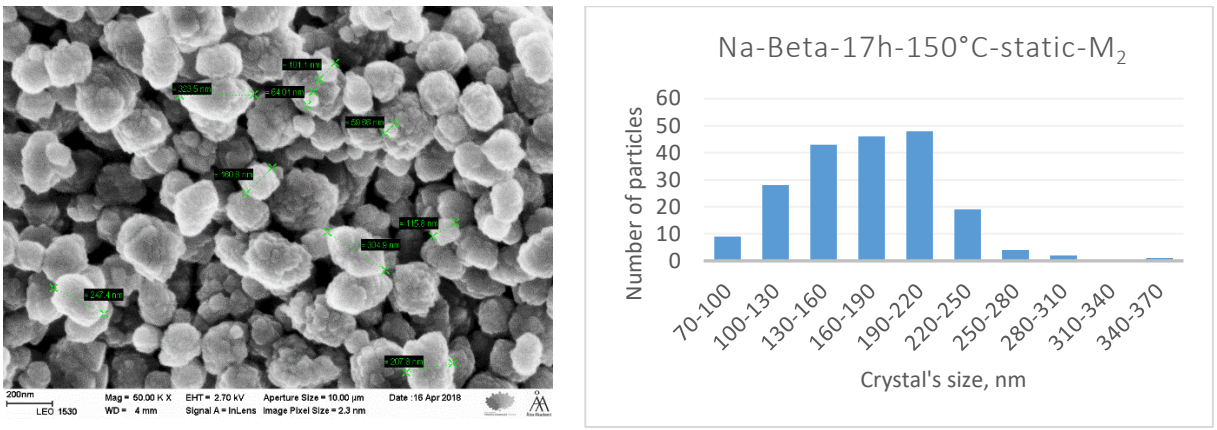

Figure 20 – Scanning Electron Micrograph of Na-Beta-17h-150 °C-static-M_2

Predominant crystal size: 190 nm.

Average particle size: 172 nm.

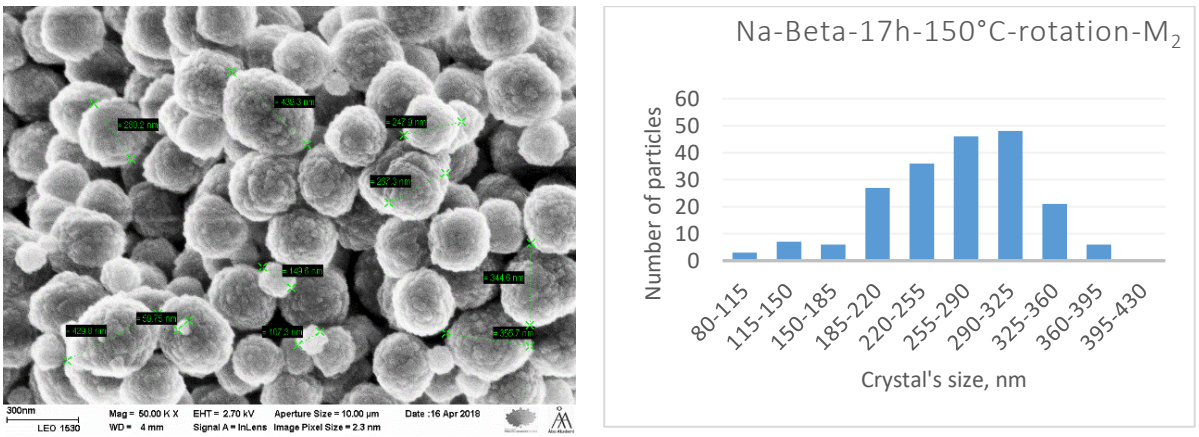

Figure 21 – Scanning Electron Micrograph of Na-Beta-17h-150 °C-rotation-M_2.

Predominant crystal size: 290 nm.

Average particle size: 263 nm.

Similar results were obtained when the synthesis time was increased from 12 h to 17 h, Figures 20, 21.

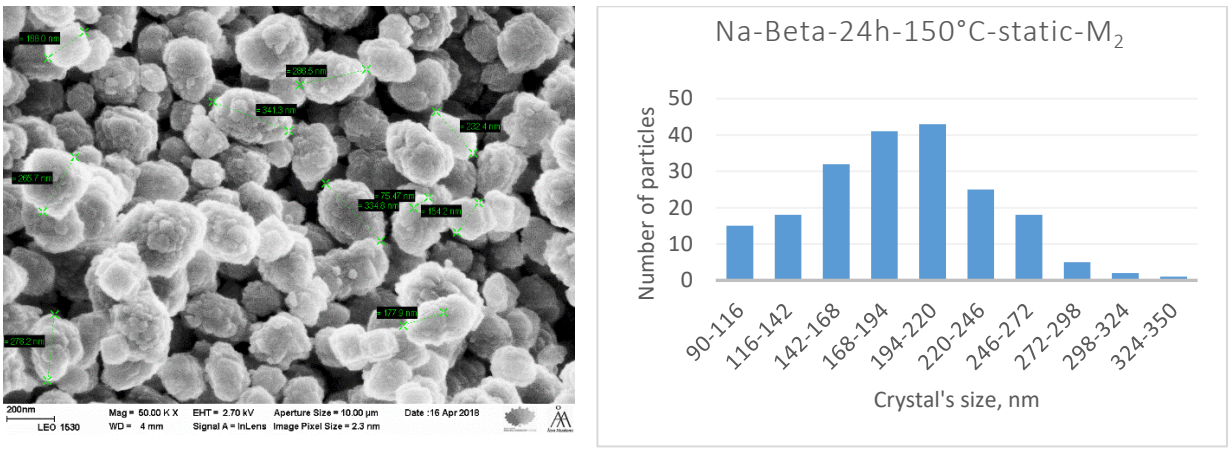

Figure 22 – Scanning Electron Micrograph of Na-Beta-24h-150 °C-static-M_2.

Predominant crystal size: 194 nm.

Average particle size: 190 nm.

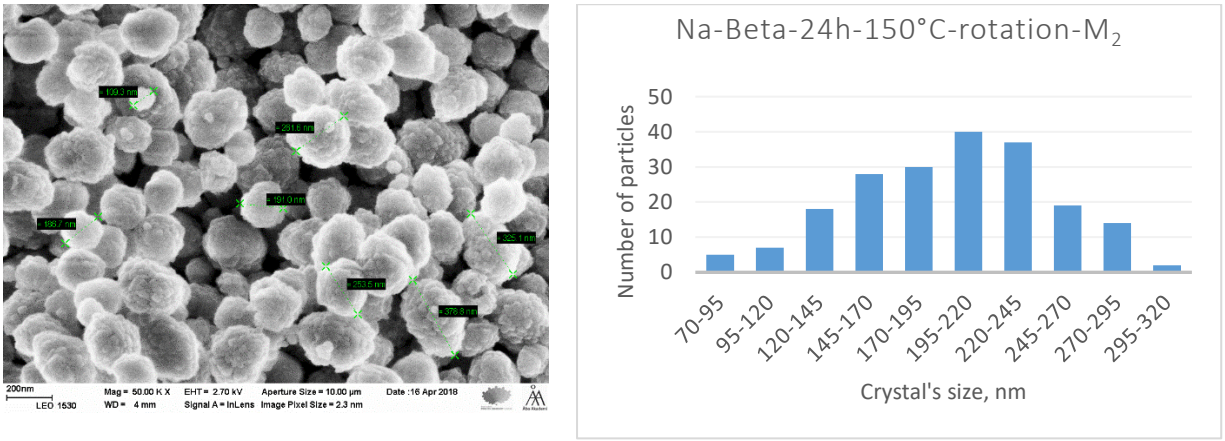

Figure 23 – Scanning Electron Micrograph of Na-Beta-24h-150 °C-rotation-M_2.

Predominant crystal size: 208 nm.

Average particle size: 199 nm.

It is important to mention here that further increase of synthesis time from 12 to 24 h at 150 °C, gave a larger average crystal size (199 nm), in the rotation mode compared to the static one (190 nm), Figure 22-23. However, an increase in the crystallite size (199 nm) was lower for synthesis time of 17 h, 150 °C (263 nm).

Figures 18-25 illustrate that changes of hydrothermal synthesis parameters led to the formation of different types of Beta zeolite structure. Moreover, an increase in the synthesis time from 12 h to 17 h and application of the rotation mode of stirring promote formation of more clearly defined spherical structures and larger crystal sizes. For example, the size of particles of Na-Beta-12h-150 °C-static-M_2 is 41 nm, while for Na-Beta-17h-150 °C-rotation-M_2 this

parameter is equal to 263 nm. In addition, an increase in temperature from 135 °C to 150 °C also positively affected the hydrothermal synthesis.

Figures 24 and 25 displays SEM of the Beta samples, that were subjected to the gel ripening procedure.

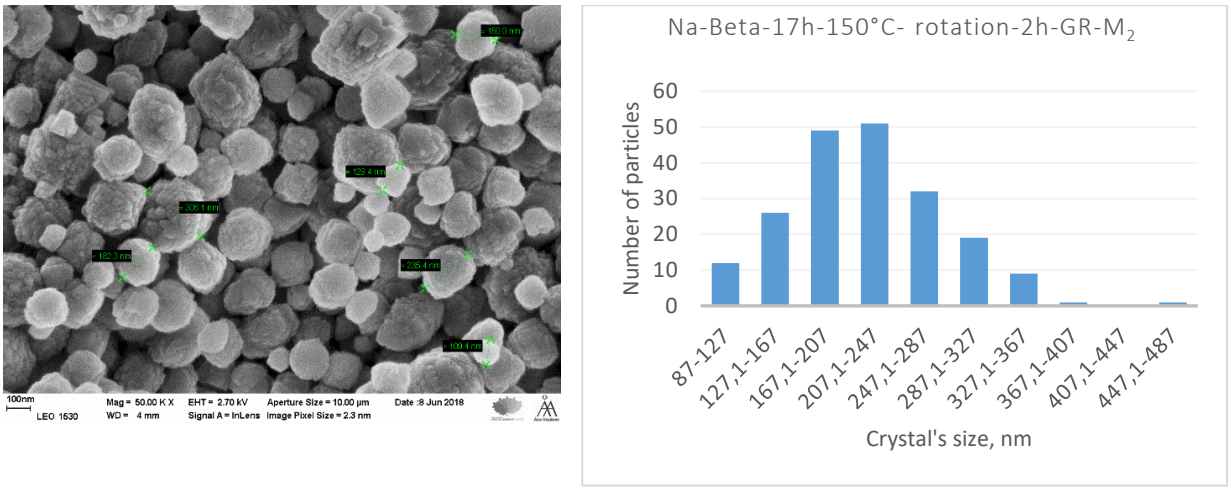

Figure 24 – Scanning Electron Micrograph of Na-Beta-17h-150 °C- rotation-2h-GR-M_2.

Predominant crystal size: 207 nm.

Average particle size: 223 nm.

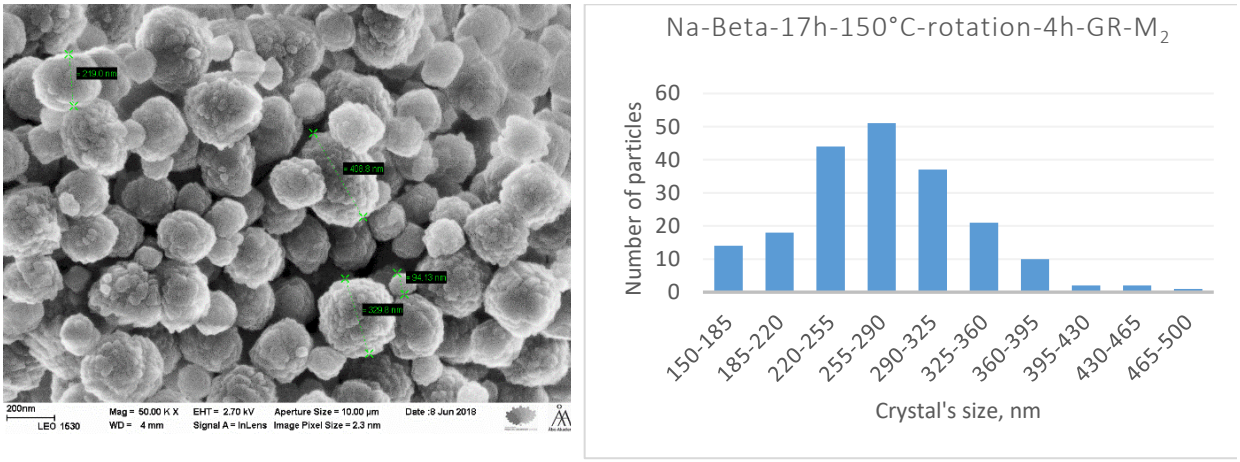

Figure 25 – Scanning Electron Micrograph of Na-Beta-17h-150 °C-rotation-4h-GR-M_2.

Predominant crystal size: 273 nm.

Average particle size: 275 nm.

According to SEM, gel ripening increase to a minor extent the crystal size of the Beta catalyst. The size of particles in Na-Beta-17h-150 °C-rotation-M_2 was equal 263 nm, while after 4h of gel ripening it has marginally increased to 275 nm.

Scanning electron micrographs of Na-Beta synthesized in 175 °C using the second method of preparation are given in Figures 26-31. The largest average crystal size (275 nm) was obtained for Beta zeolite synthesized with gel ripening at 4 h after 17 h at hydrothermal synthesis at 150 °C in rotation mode. This Beta zeolite also exhibited the highest surface area (762 m^2/g), clearly indicating the significance of the gel ripening step during the Beta zeolite synthesis. Duration of gel ripening (2 h vs.4 h) also influenced the crystal size of Beta zeolite. Thus, gel ripening for 2 h for Beta zeolite synthesis resulted in a decrease of the average crystal size (223 nm) compared to the average crystal size (275 nm) for gel ripening duration of 4 h, Figures 24, 25.

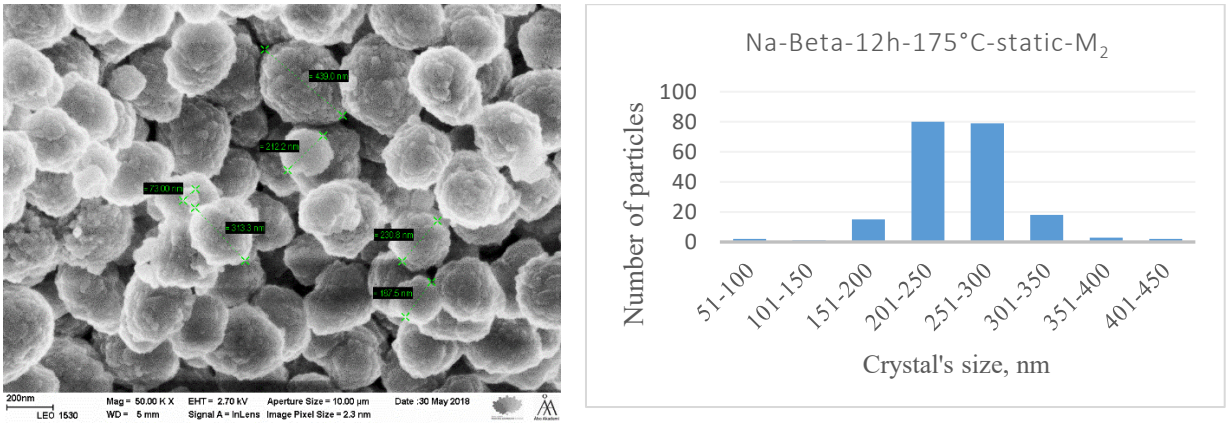

Figure 26 – Scanning Electron Micrograph of Na-Beta-12h-175 °C-static-M_2.

Predominant crystal size: 250 nm.

Average particle size: 253 nm.

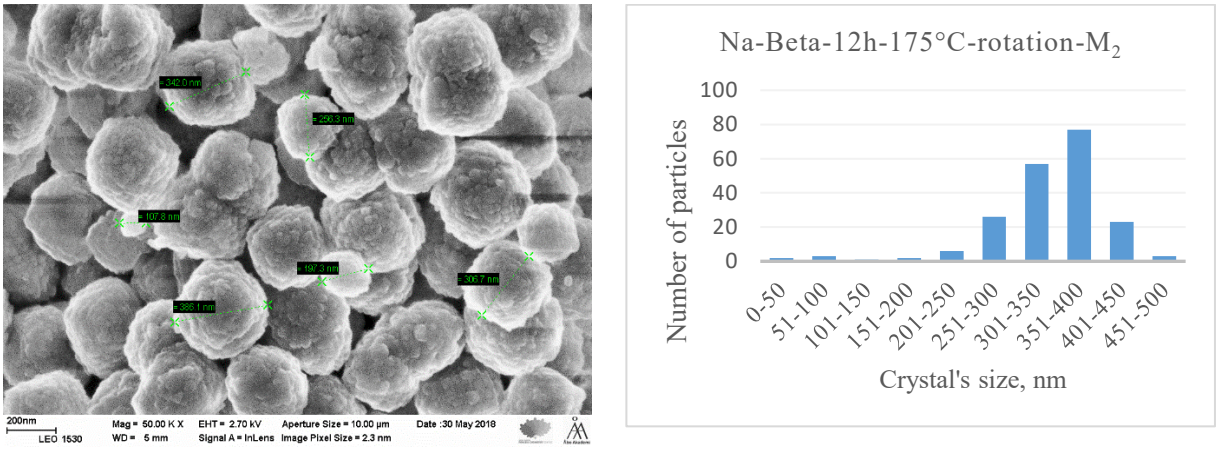

Figure 27 – Scanning Electron Micrograph of Na-Beta-12h-175 °C-rotation-M_2.

Predominant crystal size: 376 nm.

Average particle size: 340 nm.

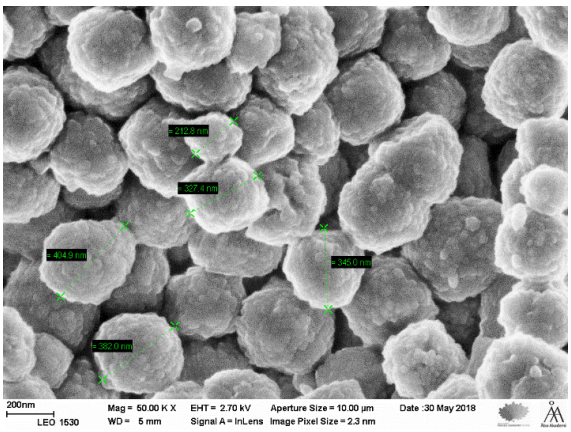

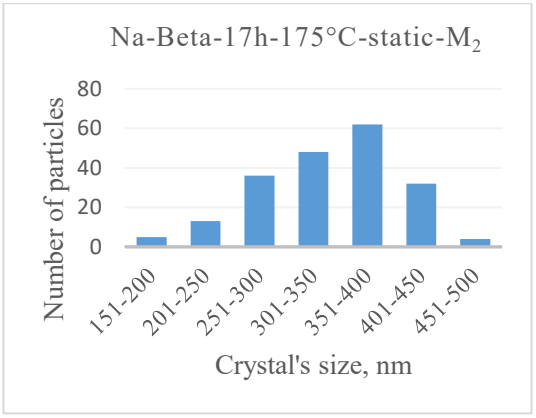

Figure 28 – Scanning Electron Micrograph of Na-Beta-17h-175 °C-static-M_2.

Predominant crystal size: 376 nm.

Average particle size: 312 nm.

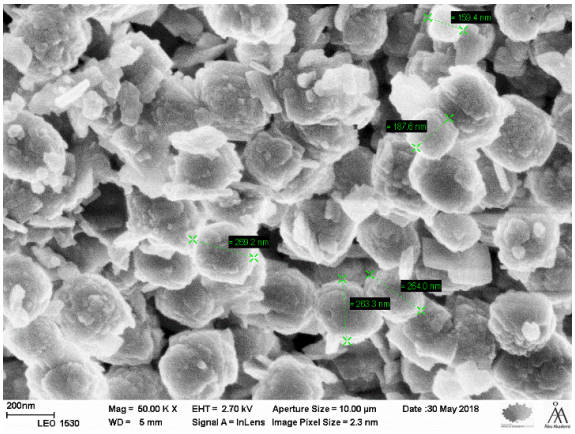

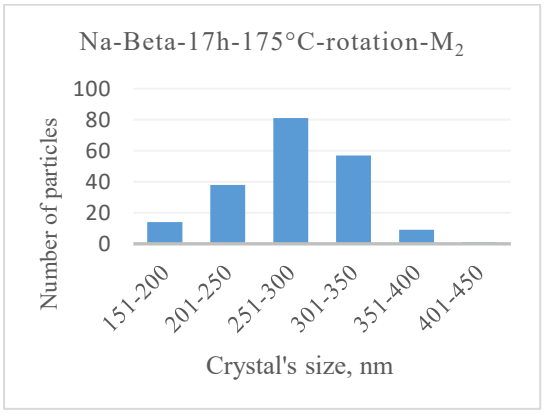

Figure 29 – Scanning Electron Micrograph of Na-Beta-17h-175 °C-rotation-M_2.

Predominant crystal size: 276 nm.

Average particle size: 338 nm.

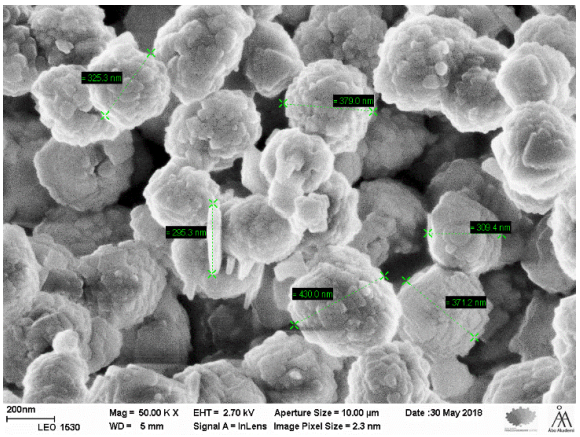

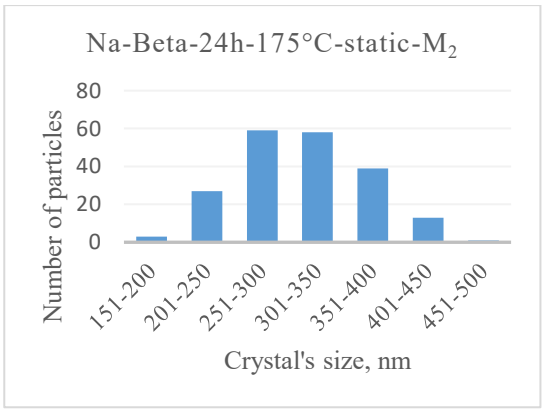

Figure 30 – Scanning Electron Micrograph of Na-Beta-24h-175 °C-static-M_2

Predominant crystal size: 300 nm.

Average particle size: 277 nm.

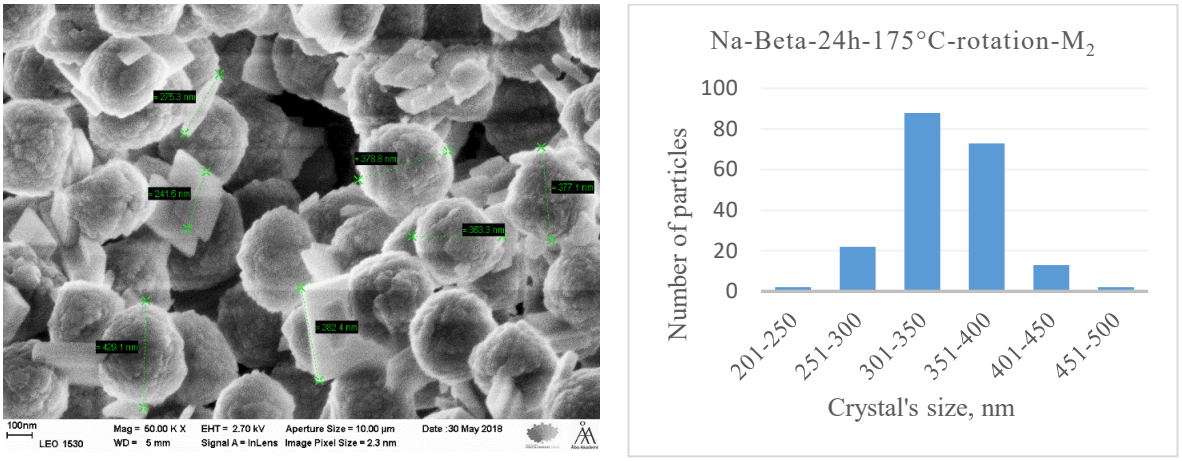

Figure 31 – Scanning Electron Micrograph of Na-Beta-24h-175 °C-rotation-M_2.

Predominant crystal size: 326 nm.

Average particle size: 344 nm.

Beta zeolite synthesis was studied at 175 °C for a duration of 12, 17, 24 h in the rotation and static modes. The highest temperature 175 °C for Beta zeolite synthesis resulted in the largest average crystal size (344 nm) for synthesis time at 24 h in the rotation mode (Figures 26-31). It is important to mention that even synthesis time 12 h and the rotation mode resulted in large average crystals (340 nm). A plausible explanation for such large average crystal size at the elevated temperature of 175 °C, could be the effect of the temperature and mode of stirring on crystallization. Even the static mode at 12 h synthesis and at 175 °C resulted in a much larger crystal size (253 nm). It should be mentioned that synthesis at 150 °C for 12 h in the static mode showed an average crystal size of just 23 nm (Figure 9). Hence, it can be concluded that synthesis parameters such as temperature, time and mode of stirring have a very significant influence on the formation of Beta zeolite structure, phase purity and crystal size formation. The surface area of the Beta zeolite synthesized at 175 °C, with varying synthesis time 12, 17 and 24 h was ranging between 535 and 701 m^2/g (Table 5). The highest surface area (701 m^2/g) was determined for Beta zeolite after 12 h of synthesis at 175 °C in the rotation mode.

In these experiments, the influence of time, stirring time, is also clearly observed. In all material synthesized at 175 °C in the rotation mode, higher values of crystal size and better crystallinity were observed.

4.2.3 Energy dispersive X-ray micro-analysis

Elemental composition of the the synthesized catalysts was evaluated using energy dispersive X-ray micro-analysis (Table 6).

Table 6 – Energy dispersive X-ray micro-analysis results

	Synthesis conditions		O	Na	Al	Si	K	Ca	Si/Al ratio
Na-Beta-M_1	12 h	150°-S	52.55	0.78	3.59	43.08	-	-	12
	24 h		52.15	1.22	4.57	41.70	-	0.36	9
	144 h		52.82	0.68	1.61	44.90	-	-	28
Na-Beta-M_2	12 h	135°-S	49.98	1.95	5.28	38.35	4.44	-	7
	17 h		50.02	2.50	4.56	38.85	4.07	-	9
	24 h		52.19	1.19	2.08	43.66	0.89	-	21
	12 h	135°-R	50.04	1.49	5.47	38.36	4.65	-	7
Na-Beta-M_2	17 h		50.19	1.48	5.58	38.49	4.27	-	7
	24 h		47.82	3.57	7.36	33.87	7.05	-	5
	12 h	150°-S	49.89	1.76	5.35	38.21	4.79	-	7
	17 h		52.56	0.52	3.28	43.36	0.28	-	13
	24 h		52.25	0.94	3.63	42.65	0.52	-	12
	12 h	150°-R	68.25	0.55	2.26	28.71	0.23	-	13
	17 h		52.75	0.45	2.93	43.87	-	-	15
	24 h		52.33	0.99	2.64	43.46	0.58	-	16
	17 h	150°-R-GR-2h	52.76	-	3.09	43.84	0.31	-	14
		150°-R-GR-4h	52.73	-	2.82	44.00	0.45	-	16
	12 h	175°-S	52.45	0.81	2.53	43.73	0.48	-	17
	17 h		52.78	-	2.69	44.16	0.36	-	16
	24 h		52.38	0.82	3.13	43.19	0.48	-	14
	12 h	175°-R	52.52	0.86	2.62	43.75	0.25	-	17
	17 h		52.33	1.15	1.93	43.96	0.63	-	23
	24 h		52.12	1.45	2.26	43.41	0.77	-	19

From the data obtained by EDX analysis, it is clear that all Beta samples have a high content of silicon and aluminum in their composition. This content is changing depending on the preparation method and synthesis parameters. In addition to aluminum and silicon such elements as sodium, potassium and calcium were also present.

4.2.4 Transmission electron microscopy

Structure, pore size, along with periodicity of the pores were studied by transmission electron microscopy as discussed in this section.

4.2.4.1 Na-Beta zeolite synthesis, first method

A transmission electron micrograph of Na-Beta-144h-150 °C-static-M_1 is presented in Figure 32.

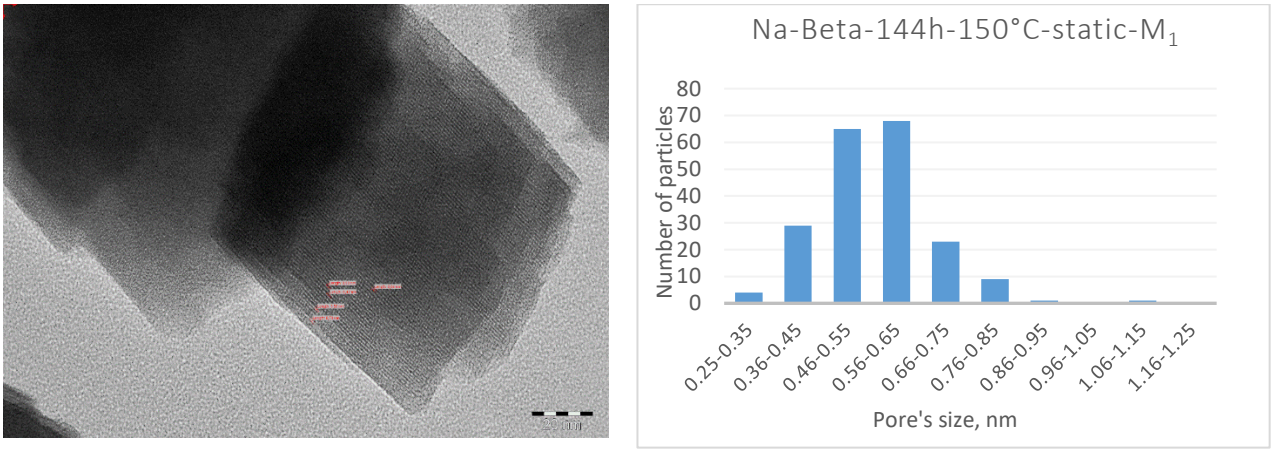

Figure 32 – Transmission electron micrograph of Na-Beta-144h-150 °C-static-M_1

Predominant pore size: 0.61 nm.

Average pore size: 0.56 nm.

The transmission electron micrographs exhibited the presence of uniform pores with a regular development of porosity and periodicity of pores. The average pore size measured for Na-Beta-144 h-150 °C-static-M_1 Beta zeolite was 0.56 nm (Figure 32).

4.2.4.2 Na-Beta zeolite synthesis, second method

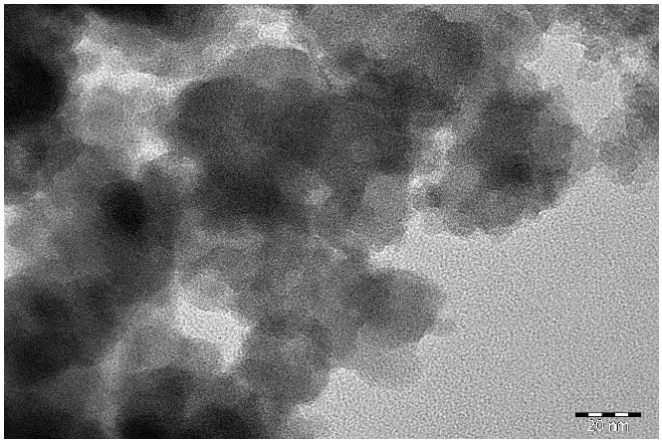

Figure 33 – Transmission electron micrograph of Na-Beta-12h-135 °C-rotation-M_2

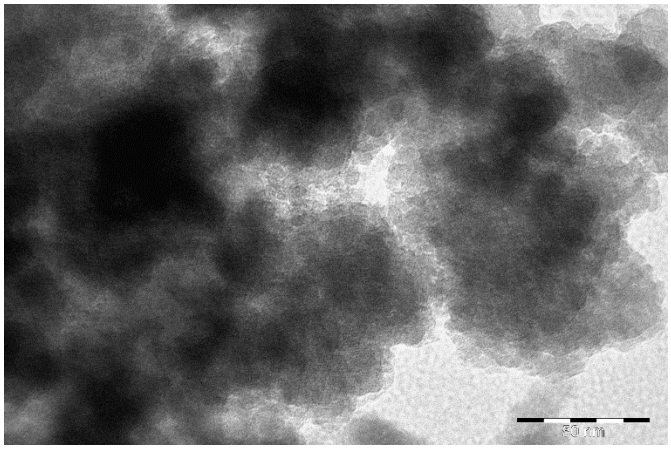

Figure 34 – Transmission electron micrograph of Na-Beta-17h-135 °C-rotation-M_2

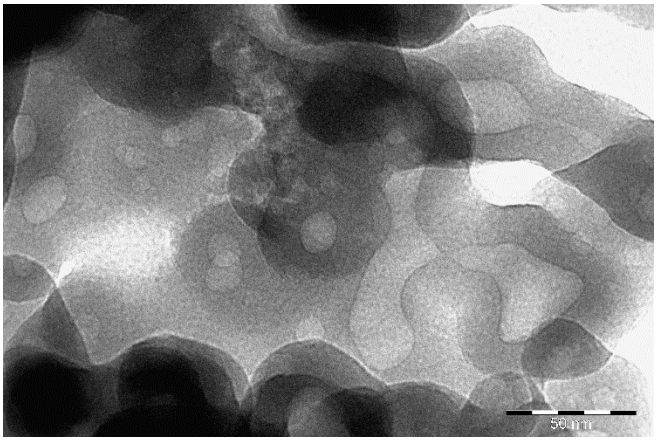

Figure 35 – Transmission electron micrograph of Na-Beta-24h-135 °C-rotation-M_2

All samples synthesized at 135 °C did not give promising results not displaying a uniform porous structure or the channel system.

Figures 36-41 show the results of TEM analysis of materials, which were synthesized at 150 °C and different types of stirring (rotation and static).

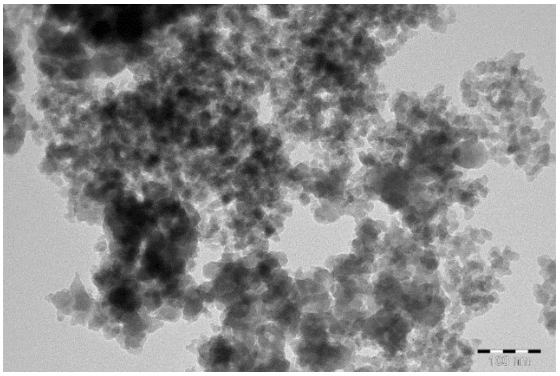

Figure 36 – Transmission electron micrograph of Na-Beta-12h-150 °C-static-M_2

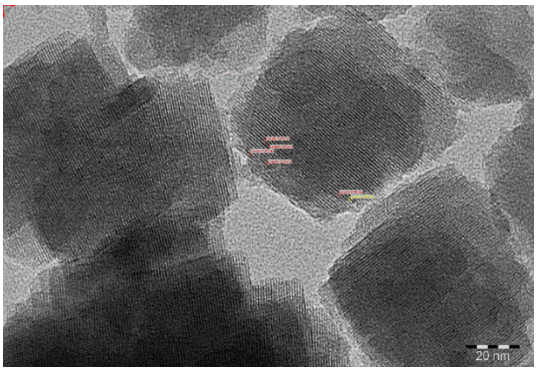

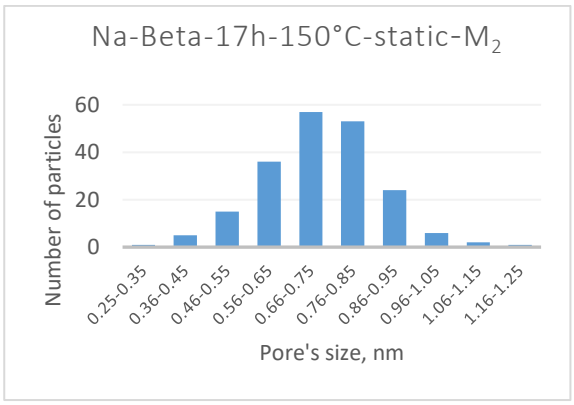

Figure 37 – Transmission electron micrograph of Na-Beta-17h-150 °C-static-M_2.

Predominant pore size: 0.71 nm.

Average pore size: 0.73 nm.

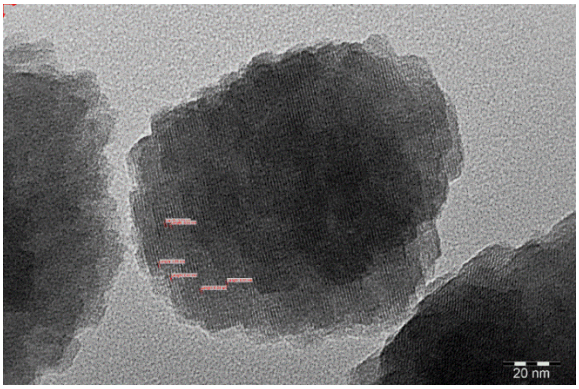

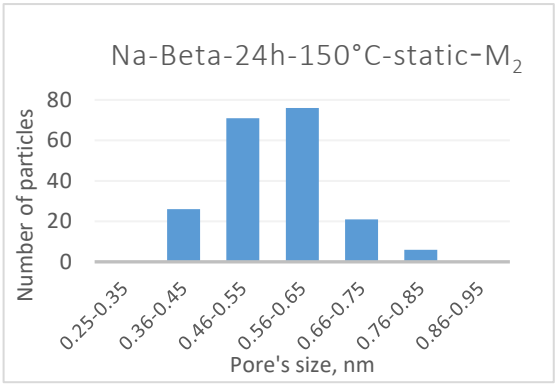

Figure 38 – Transmission electron micrograph of Na-Beta-24h-150 °C-static-M_2.

Predominant pore size: 0.56 nm.

Average pore size: 0.55 nm.

The pore size measured from the transmission electron micrographs of Na-Beta-17 h-150 °C-static-M_2 and Na-Beta-17 h-150 °C-rotation-M_2 zeolites, showed a larger pore size (0.73 nm) for the static mode of synthesis than for the rotation one (0.55 nm), Figures 37 and 38. Hence, it was inferred that the method of stirring influenced the pore size formation. Beta zeolite synthesized using both methods of stirring showed typical crystal shapes of Beta zeolite. The X-ray powder diffraction also confirmed the presence of typical structures of Beta zeolite for Na-Beta-17 h-150 °C-static-M_2 and Na-Beta-17 h-150 °C-rotation-M_1.

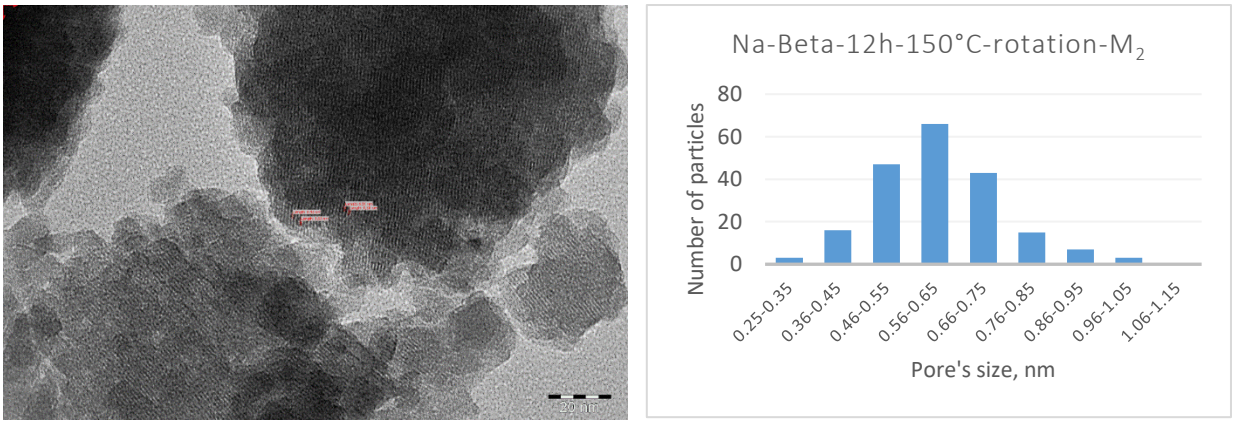

Figure 39 – Transmission electron micrograph of Na-Beta-12h-150 °C-rotation-M_2.

Predominant pore size: 0.61 nm.

Average pore size: 0.61 nm.

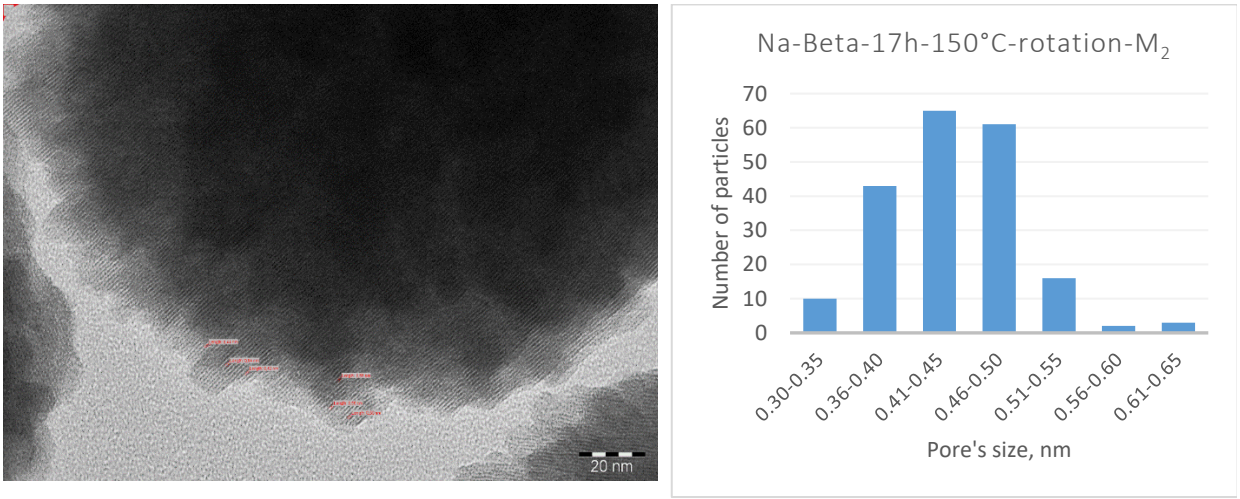

Figure 40 – Transmission electron micrograph of Na-Beta-17h-150 °C-rotation-M_2.

Predominant pore size: 0.45 nm.

Average pore size: 0.44 nm.

It is significant to mention that an increase in the synthesis time from 12 h to 17 h for hydrothermal synthesis at 150 °C in the rotation mode resulted in a decrease in the average pore size 0.44 nm

for Na-Beta-17h-150 °C-rotation-M_2 in comparison with the Na-Beta-12h-150 °C-rotation-M_2 (0.61 nm), Figures 39, 40.

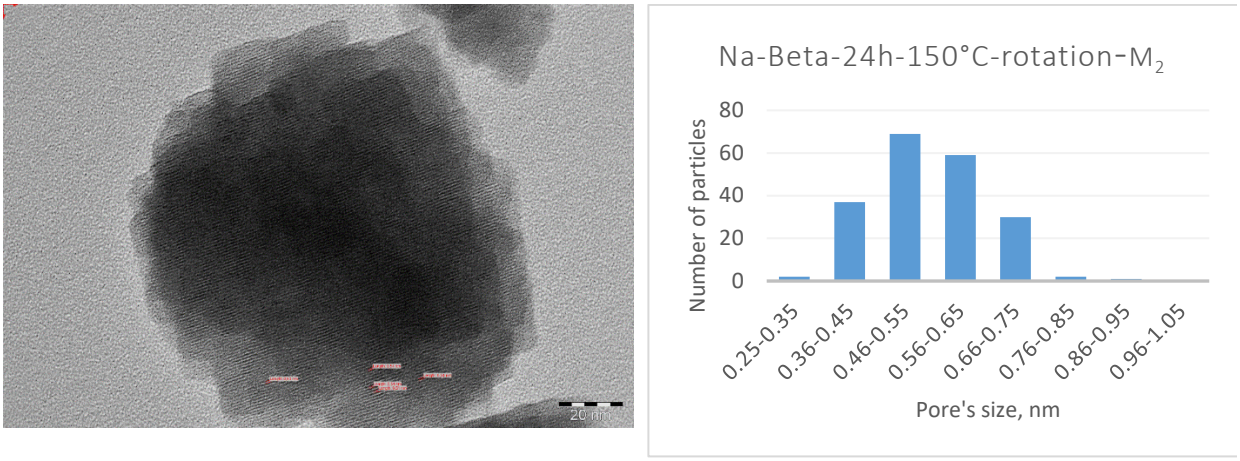

Figure 41 – Transmission electron micrograph of Na-Beta-24h-150 °C-rotation-M_2

Predominant pore size: 0.51 nm.

Average pore size: 0.55 nm.

Almost all catalysts, except for the Na-Beta-12h-150 °C-static-M_2, had a well-developed system of pores and channels. Probably 12 hours were not sufficient to form pores.

In addition, the influence of gel ripening was investigated.

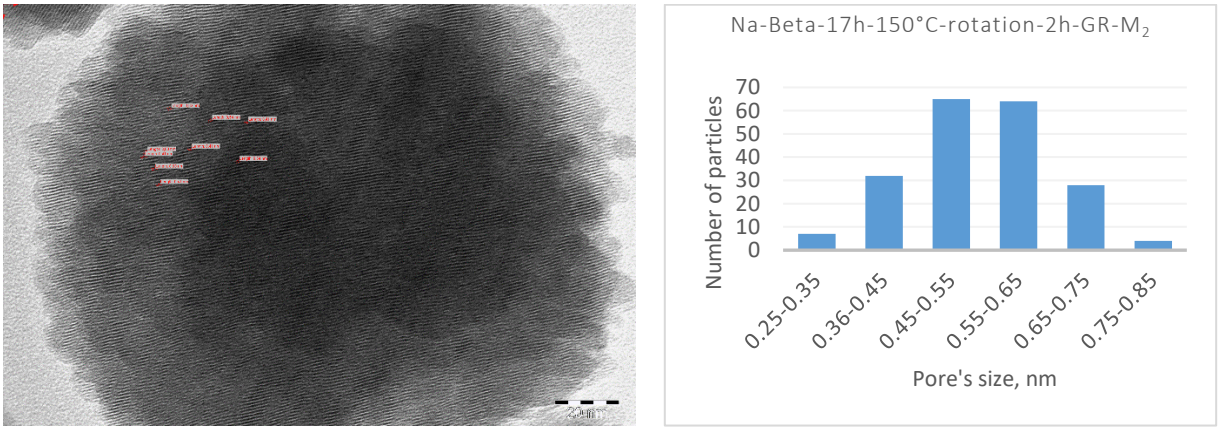

Figure 42 – Transmission electron micrograph of Na-Beta-17h-150 °C-rotation-2h-GR-M_2.

Predominant pore size: 0.55 nm.

Average pore size: 0.54 nm.

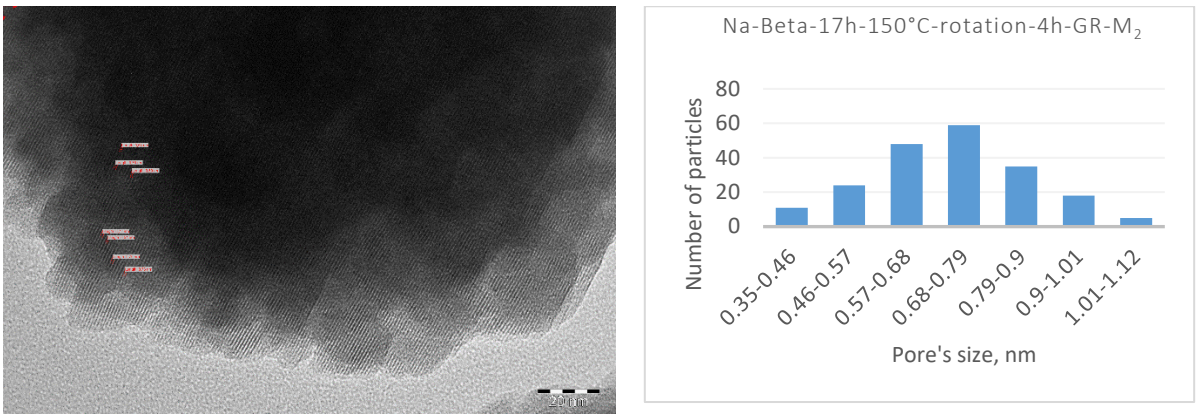

Figure 43 – Transmission electron micrograph of Na-Beta-17h-150 °C-rotation-4h-GR-M_2.

Predominant pore size: 0.74 nm.

Average pore size: 0.71 nm.

Na-Beta-17h-150 °C-rotation-2h-GR-M_2 and Na-Beta-17h-150 °C-rotation-4h-GR-M_2 zeolites synthesized with varying gel ripening methods showed an increase in the average pore size (0.71 nm) for 4 h ripening in comparison with 2 h of gel ripening. Taking into consideration above mentioned results from the gel ripening experiments, it can be concluded that the method of gel ripening and its duration influenced the average pore size. In particular gel ripening increases the pore size. The average pore size of Na-Beta-17h-150 °C-rotation-M_2 is 0.44 nm, however after 2h of gel ripening it increased to 0.54 and after 4h further to 0.71 nm.

Furthermore, Beta zeolite catalysts synthesized at 175 °C were also studied by transmission electron microscopy. The results of TEM are shown in Figures 44-46.

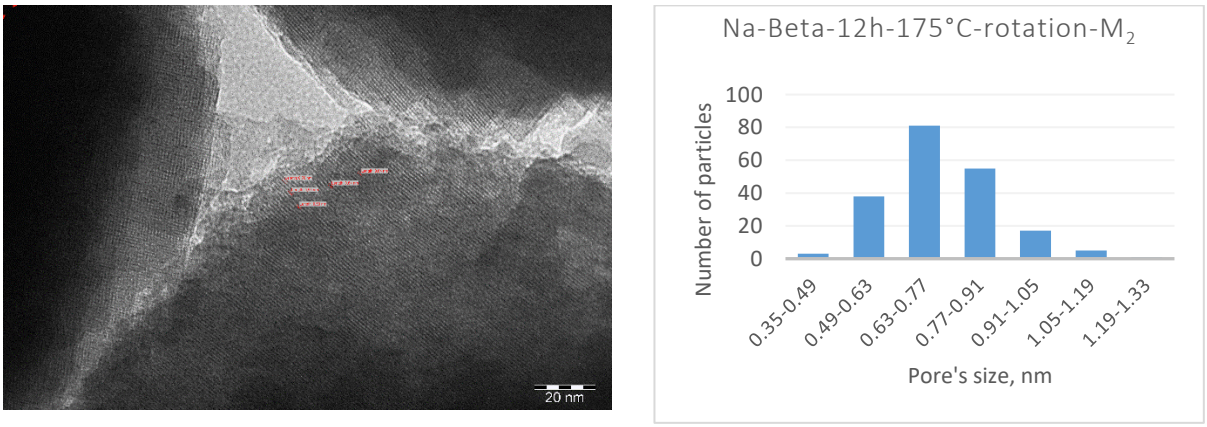

Figure 44 – Transmission electron micrograph of Na-Beta-12h-175 °C-rotation-M_2.

Predominant pore size: 0.70 nm.

Average pore size: 0.74 nm.

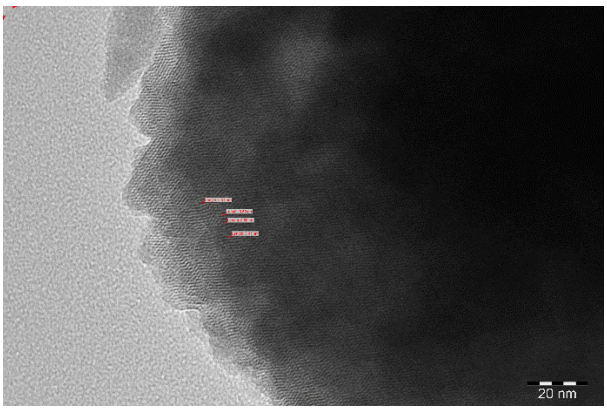

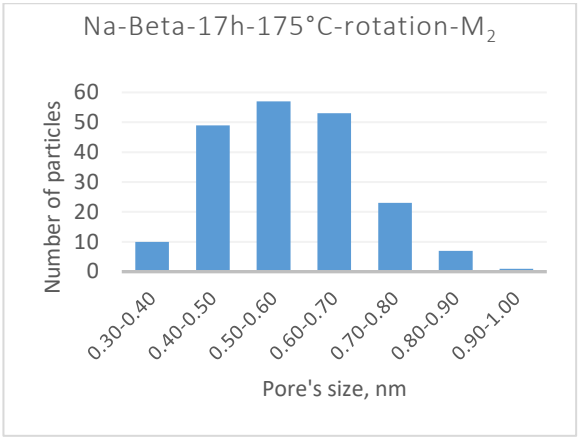

Figure 45 – Transmission electron micrograph of Na-Beta-17h-175 °C-rotation-M_2.

Predominant pore size: 0.55 nm.

Average pore size: 0.58 nm.

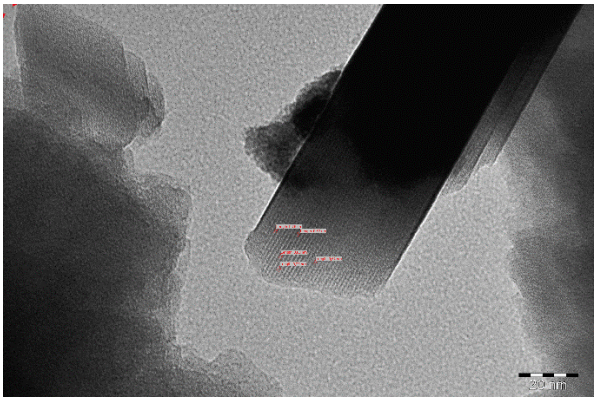

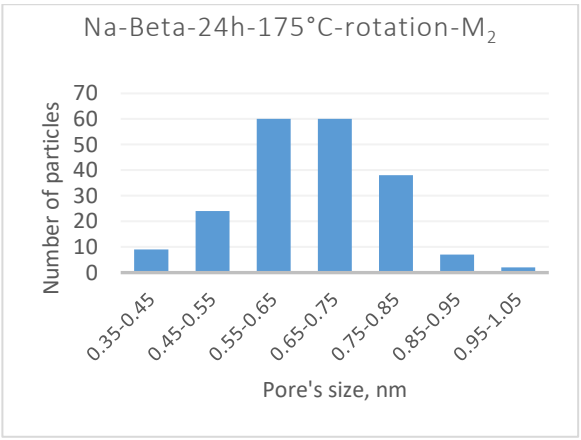

Figure 46 – Transmission electron micrograph of Na-Beta-24h-175 °C-rotation-M_2.

Predominant pore size: 0.65 nm.

Average pore size: 0.66 nm.

Na-Beta zeolite synthesized at the highest temperature of 175 °C under the rotation mode with varying synthesis time 12, 17, 24 h exhibited an average pore size of 0.74, 0.58 and 0.66 nm, respectively, Figures 44-46. All Beta zeolite samples showed uniform pores, porosity and periodicity of pores. It is important to mention that the average crystal sizes of Beta zeolites synthesized at 175 °C were also very large (253-344 nm). The X-ray powder diffraction patterns showed the presence of Beta zeolite.

TEM results of catalysts prepared at 175 °C in the rotation mode confirm that all catalyst possess have well-developed pore and channel systems.

4.2.5 X-ray powder diffraction

The structure, phase purity and crystallinity of all the Beta zeolite catalysts were identified using X-ray powder diffractometer. The results of the XRD measurements are shown in Table 7.

The estimated average crystal sizes d_c for the measured samples, based on the Rietveld refinements. The quality of the Rietveld refinement fit is described by the parameter R_{exp}, where a smaller R_{exp} indicates a better fit to the measured data.

Table 7 – XRD results

№	Sample	Observed phase (framework)	d_c[Å]	R_{exp} [%]
1	Na-Beta-12h-150 °C-static-M_1	-	–	–
2	Na-Beta-24h-150 °C-static-M_1		–	–
3	Na-Beta-144h-150 °C-static-M_1	Beta zeolite polymorph A	160±30	2.72
4	Na-Beta-12h-135 °C-rotation-M_2	–	–	–
5	Na-Beta-17h-135 °C-rotation-M_2	Beta zeolite polymorph A	n/a	–
6	Na-Beta-24h-135 °C-rotation-M_2	–	–	–
7	Na-Beta-12h-150 °C-rotation-M_2	Beta zeolite polymorph A	160±20	2.69
8	Na-Beta-17h-150 °C-rotation-M_2		170±30	2.71
9	Na-Beta-24h-150 °C-rotation-M_2		170±20	2.75
10	Na-Beta-12h-175 °C-rotation-M_2			2.78
11	Na-Beta-17h-175 °C-rotation-M_2			2.70
12	Na-Beta-24h-175 °C-rotation-M_2	Beta zeolite polymorph A, unidentified phase	160±20 n/a	2.75 n/a
13	Na-Beta-17h-150 °C-rotation-2h-GR-M_2	Beta zeolite polymorph A	170±20	2.82
14	Na-Beta-17h-150 °C-rotation-4h-GR-M_2			2.89

Catalysts prepared using the first method of hydrothermal treatment were studied by XRD. Materials Na-Beta-12h-150 °C-static-M_1 and Na-Beta-24h-150 °C-static-M_1 were amorphous. Thus, the beta zeolite structure was not present in the samples or their concentrations were too small to be detected. Diffractogram of Sample Na-Beta-144h-150 °C-static-M_1 consisted of peaks related to beta zeolite polymorph A. The crystal size based on the Rietveld refinement method was 160 ± 30 Å.

The plausible explanation for the absence of Beta zeolite structure was the insufficient time and the static mode of synthesis for the formation of the Beta zeolite phase. The measured diffractograms are presented in Figures 47-49.

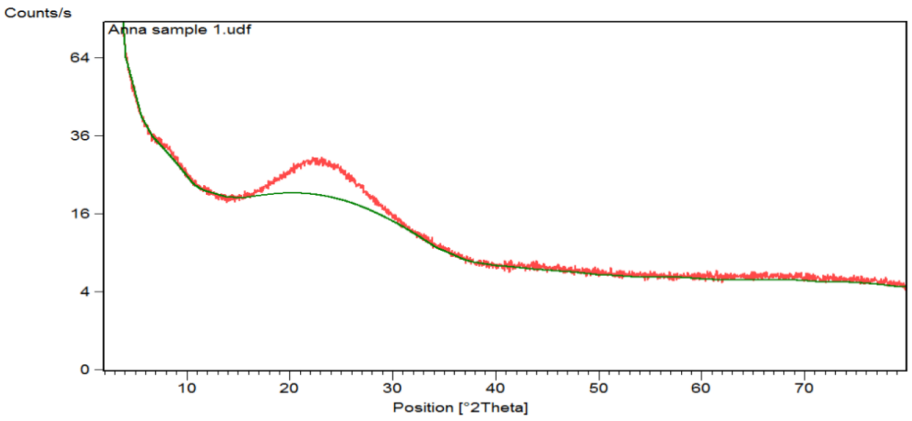

Figure 47 – The X-ray powder diffraction patterns of Na-Beta-12 h-150 °C-static-M_1 zeolite.

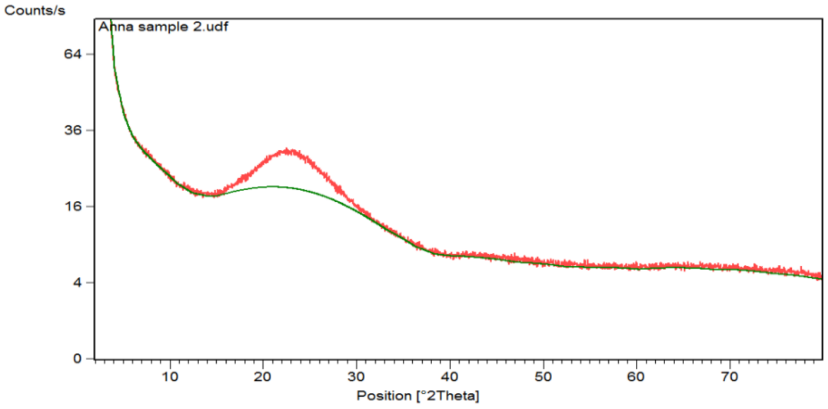

Figure 48 – The diffractogram of Na-Beta-24 h-150 °C-static-M_1

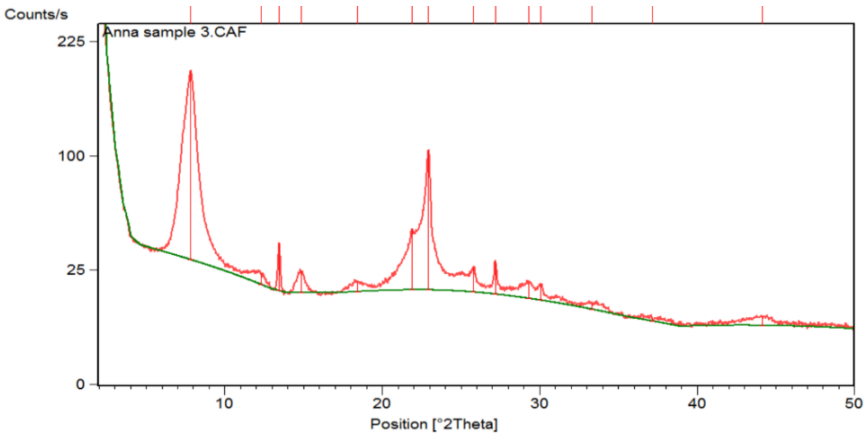

Figure 49 – The diffractogram of Na-Beta-144 h-150 °C-static-M_1

Similar results were observed for Na-Beta-12h-135 °C-rotation-M_2 and Na-Beta-24h-135 °C-rotation-M_2, Figures 50, 51.

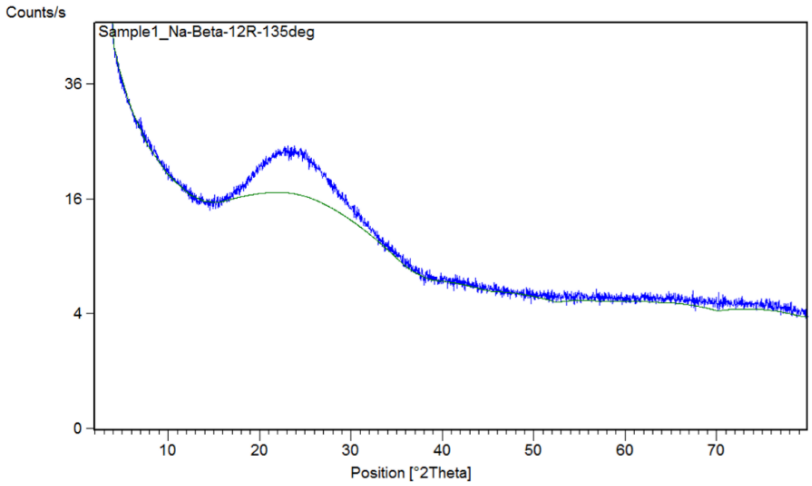

Figure 50 – The diffractogram of Na-Beta-12h-135 °C-rotation-M_2

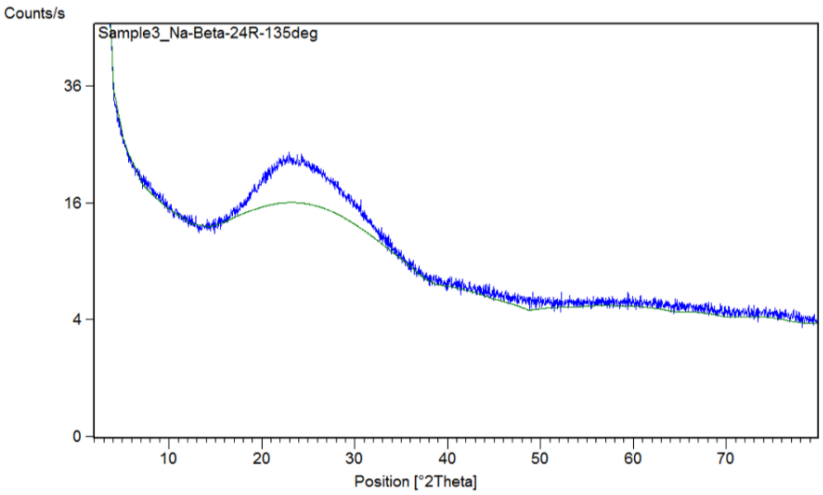

Figure 51 – The diffractogram of Na-Beta-24h-135 °C-rotation-M_2

In the diffractogram of Na-Beta-17h-135 °C-rotation-M_2, three broad diffraction peaks with low intensity related to Beta zeolite [46] were observed. It can be concluded that the crystallinity of the sample was low, but the sample was not completely amorphous. The diffractogram is presented in Figure 52. The Rietveld refinement method was used to estimate the crystal size d_c, however the attempt was unsuccessful.

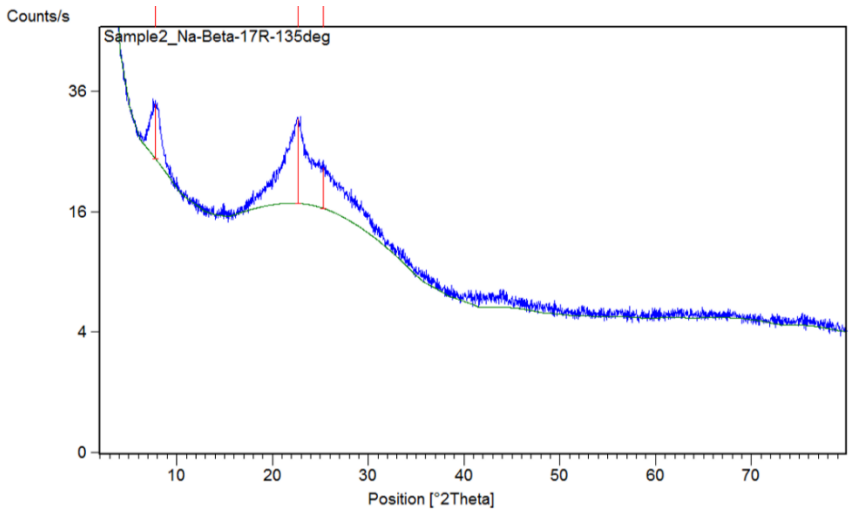

Figure 52 – The diffractogram of Na-Beta-17h-135 °C-rotation-M_2

In all samples, prepared by the second method at 150 °C and 175 °C in the rotation mode, the diffraction peaks related to the structure of Beta zeolite [46] were observed. A typical diffractogram and the Rietveld refinement method for estimation of the crystal size d_c are presented in Figure 53:

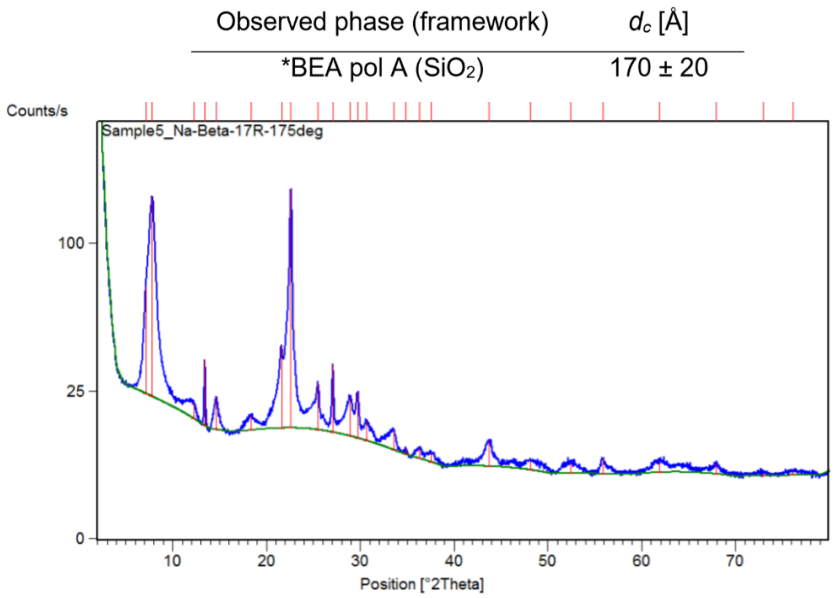

Figure 53 – The diffractogram of Na-Beta-17h-175 °C-rotation-M_2

An interesting case was Na-Beta-24h-175 °C-rotation-M_2. For this material, unidentified diffraction peaks (relatively high and narrow) were observed at 2θ = 6.1°, 2θ = 18.5°, 2θ = 21.2°, and 2θ = 24.9°, and they are related to unidentified phase(s). These peaks were observed only with this sample (Figure 54).

The Rietveld refinement method was used to estimate the crystal size d_c of the beta zeolite phase. The analysis resulted in the following values:

Observed phase (framework)	d_c [Å]
*BEA pol A (SiO_2)	160 ± 20

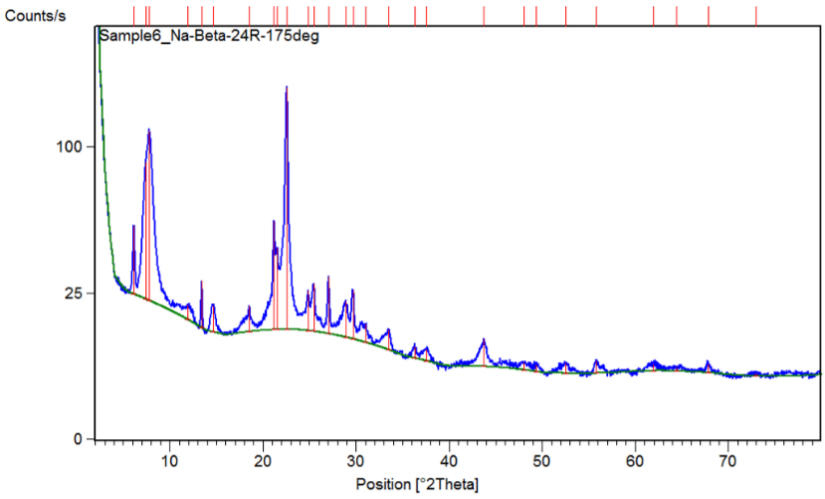

Figure 54 – The measured diffractogram of Na-Beta-24h-175 °C-rotation-M_2

4.2.6 ^{29}Si and ^{27}Al MAS NMR spectrometry

The synthesized Beta zeolite samples were studied for the presence of Al in the framework and extra-framework.

Six H-Beta zeolite samples have been studied:

No_1: H-Beta-12h-static-150 °C-M_2
No_2: H-Beta-17h-static-150 °C-M_2
No_3: H-Beta-24h-static-150 °C-M_2
No_4: H-Beta-12h-rotation-150 °C-M_2
No_5: H-Beta-17h-rotation-150 °C-M_2
No_6: H-Beta-24h-rotation-150 °C-M_2

Figure 60 shows ^{29}Si and ^{27}Al MAS NMR spectra of studied H-Beta zeolite samples. ^{29}Si and ^{27}Al both show almost identical spectra for all samples except the spectra for sample No1. ^{29}Si spectrum of sample No1 was fitted by three broad Gaussian lines at -108 ppm (72% of total intensity), at -100 ppm (22%) and at -92 ppm (6%). The spectrum indicates a poor long range order in this sample. The rest of ^{29}Si spectra were fitted by 5 Gaussian lines at frequencies -92 ppm

(1.4% of total intensity), -103 ppm (1.8%), broad line at -106 ppm (47%), strong line at -111 ppm (40%) and a line at -114 ppm (10%). The last two components belong to silicones in nine different T-sites of highly siliceous Beta-zeolite [48], where the two sites have chemical shift at around -115 ppm, and seven sites have chemical shift around -111 ppm. The weak line at -92 ppm belongs usually to silicon sites Q^2, where a silicon has two nearest neighbor silicones and two OH groups [49]. Similarly, the line at -103 ppm belongs to Q^3 silicon sites, where silicon has 3 nearest neighbor silicones and a single OH group. The broad line with a maximum at -106 ppm can be attributed to various silicon sites where the nearest neighbor silicon is substituted by Al. The chemical shift, Gaussian width, relative intensity of the components and the total intensities of ^{29}Si spectra in samples 1 to 6 are given in Table 7. The total intensity in ^{29}Si spectra is almost equal of samples No_3 to No_6. It is considerably smaller for the sample No_2 and much smaller for the sample No_1.

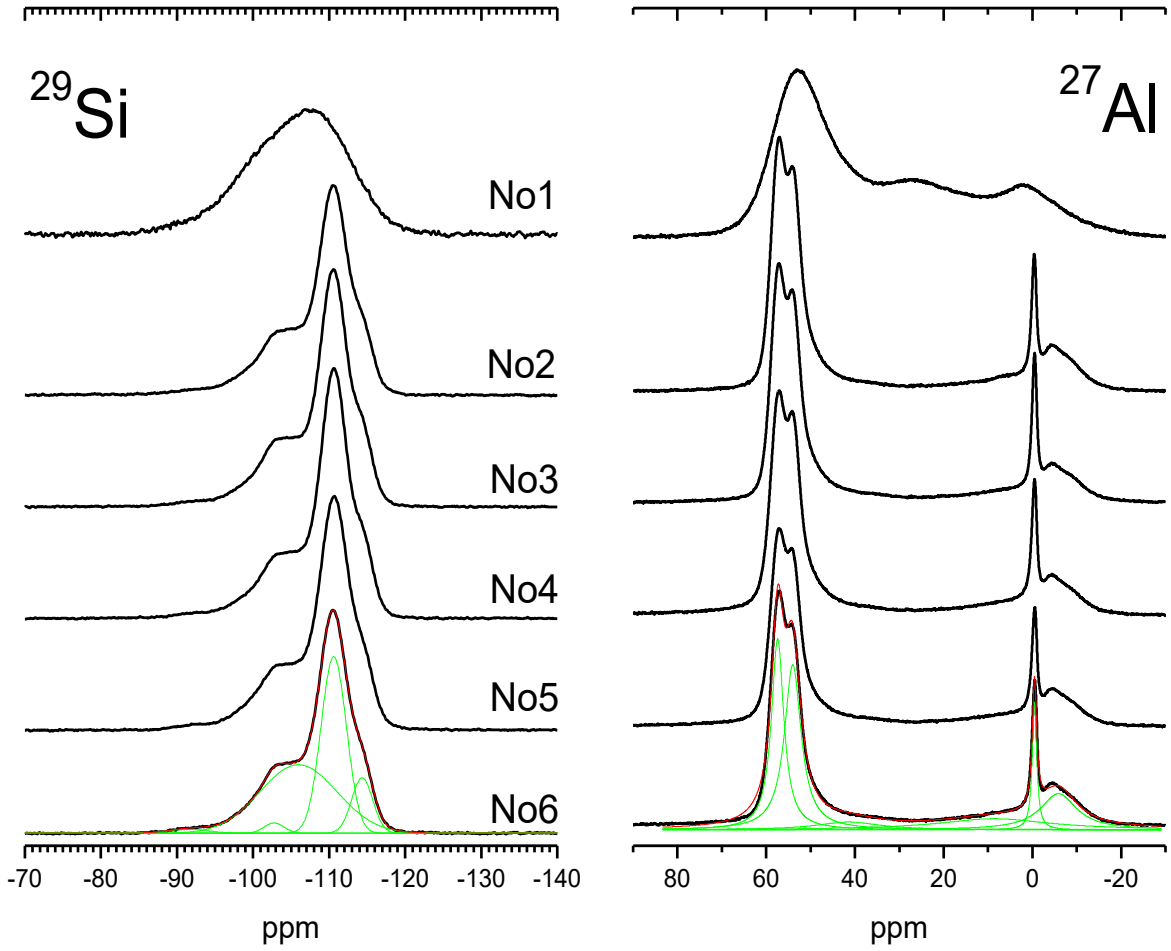

Figure 60 – ^{29}Si (left) and ^{27}Al (right) MAS NMR spectra of H-Beta zeolite samples. Decomposition of the spectrum is given for the sample No_6.

Table 7 – Parameters of the peaks in ^{29}Si MAS NMR spectra

Sample	No_2	No_3	No_4	No_5	No_6	No_1
Peak 1 (ppm)	-114.4	-114.4	-114.4	-114.5	-114.4	-108.16
Width (ppm)	2.7	2.6	2.6	2.7	2.8	9.5
Intensity (%)	10.4	10.8	10.8	9.8	10.3	72
Peak 2 (ppm)	-110.7	-110.6	-110.6	-110.7	-110.6	-100.0
Width (ppm)	3.3	3.2	3.2	3.4	3.3	7.3
Intensity (%)	40.1	41.3	41.3	42.2	39.8	22.4
Peak 3 (ppm)	-105.9	-106.0	-106.0	-106.2	-106.0	-92.3
Width (ppm)	9.8	9.9	9.9	10.5	10.1	8.1
Intensity (%)	45.5	44.1	44.1	45.1	46.8	5.70
Peak 4 (ppm)	-102.8	-102.8	-102.8	-102.7	-102.8	-
Width (ppm)	2.6	2.5	2.6	2.8	2.6	-
Intensity (%)	1.7	2.0	1.5	1.9	1.8	-
Peak 5 (ppm)	-92.2	-91.8	-91.8	-91.4	-91.5	-
Width (ppm)	8.1	6.5	6.5	4	5.2	-
Intensity (%)	2.3	1.7	1.6	1	1.4	-
Total Intensity (arb. units)	409	441	447	446	439	149

^{27}Al spectra of samples No_2 to No_6 showing typical high field MAS NMR spectra of H-Beta zeolites [50] have been fitted with 6 Lorentzian lines at 57.4 ppm (relative intensity 27%) and 54.0 ppm (32%) which belong to Al ions in tetrahedral sites T3-T9 and T1-T2, respectively [51]. The lines at -5.9 ppm (15%) and a sharp line at -0.5 ppm (6%) belong to Al ions in octahedral sites. The intensity between these two regions is accounted by two broad lines at 8 ppm (13%) and at 40 ppm (6%). Typically the broad lines appear in dehydrated samples [50]. The spectrum of the sample No 1 was simulated by three broad lines at 0 ppm (14%) at 31 ppm (45%) and 53 ppm (41%). Exact frequencies, widths, relative intensities of the lines in ^{27}Al spectra are given in Table 8 together with the total intensity in Al spectra. In Al spectra the total intensity is varied from 767 to 988 units and for sample No_1 it is considerably larger.

Table 8 – Parameters of the peaks in ^{27}Al MAS NMR spectra

Sample	No_1	No_2	No_3	No_4	No_5	No_6	Assignment
Peak 1 (ppm)	52.80	57.38	57.44	57.45	57.44	57.42	Al(IV)a
Width (ppm)	11.5	3.2	3.2	3.52	3.48	3.38	
Intensity (%)	41	27.0	26.4	28.9	27.1	27.1	

Continuation of Table 8

Sample	No1	No2	No3	No4	No5	No6	Assignment
Peak 2 (ppm)		53.92	53.99	53.97	54.04	54.01	Al(IV)b
Width (ppm)		4.5	4.4	4.34	4.49	4.53	
Intensity (%)		35.1	34.1	32.3	32.1	31.5	
Peak 3 (ppm)	0.1	-5.75	-5.90	-5.74	-5.86	-5.88	Al(VI)a
Width (ppm)	15.8	9.7	10.1	9.03	9.53	9.87	
Intensity (%)	14	16.3	14.4	13.3	15.1	15.0	
Peak 4 (ppm)		-0.38	-0.46	-0.44	-0.48	-0.48	Al(VI)b
Width (ppm)		1.2	1.2	1.27	1.23	1.19	
Intensity (%)		5.7	6.8	6.8	6.3	6.4	
Peak 5 (ppm)		9.56	9.90	7.58	8.48	8.57	
Width (ppm)		26.2	30.1	26.52	27.46	30.66	
Intensity (%)		11.3	12.8	12.9	13.2	14.3	
Peak 6 (ppm)	30.87	42.91	43.49	45.05	41.81	41.47	Al(V)
Width (ppm)	32.0	14.5	14.6	15.82	18.19	17.37	
Intensity (%)	45	4.5	5.5	5.7	6.4	5.7	
Total Intensity	1206	988	878	835	767	896	

4.2.7 Fourier transform infrared spectrometry

Experimental values of acidity for the most interesting material prepared by ion exchange of the parent sodium form (Na-Beta-17h-rotation-150 °C-M_2) were determined using FTIR (Figure 9). The probe molecule was pyridine, which was desorbed at different temperatures of 250 °C, 350 °C and 450 °C reflecting the total number of sites, medium and strong sites and finely only strong sites, respectively. Table 9 exhibits values of both Brønsted and Lewis acidity.

Table 9 – Quantification of acidity

Sample	Brønsted acid sites, μmol/g			Lewis acid sites, μmol/g			Ref.
	250°C	350°C	450°C	250°C	350°C	450°C	
H-Beta-17h-rotation-150°C-M_2	260	251	154	25	18	5	-
H-Beta-25	219	187	125	82	43	25	[52]
H-Beta-150	176	161	72	43	23	10	[53]
H-Beta-300	54	49	23	28	9	4	[52]

As can be seen from Table 9 the total number of acid sites in H-Beta-17h-rotation-150 °C-M_2 is higher than reported previously for beta zeolites with different silica to alumina ratio [52-53].

5. Conclusions

The influence of such synthesis parameters as time, pH, mode of stirring and temperature, along with an extra pre-synthesis step of gel ripening was studied using synthesis of Beta zeolite as a show case. Physico-chemical characterizations of the synthesized materials was performed using an arsenal of modern analytical methods comprising nitrogen physisorption, SEM, TEM, EDX, XRD, FTIR with pyridine as the probe molecule and ^{29}Si and ^{27}Al MAS NMR. Variation of the synthesis parameters significantly influenced the physico-chemical properties of Beta zeolite. It was observed that the rotation mode of stirring and temperature above 135 °C in hydrothermal synthesis are necessary to obtain phase pure Beta zeolites structure. Synthesized Beta zeolites exhibited a large surface area (>500 m^2/g). The highest surface area (762 m^2/g) was obtained for Na-Beta-17h-150°C-M_2-4h-GR while the second highest surface area (704 m^2/g) was present in Na-Beta-17h-150°C-M_2-2h-GR. Hence, it was concluded that gel ripening in the Beta zeolite synthesis was of immense importance for the creation of porosity, pore volume and surface area. It should be noted that the achieved result of the surface area measurement is significantly higher than reported in the literature [22, 24, 39-42].

The X-ray powder diffraction patterns of Na-Beta-144h-150°C-static-M_1, Na-Beta-12h-150 °C-rotation-M_2, Na-Beta-17h-150°C-rotation-M_2, Na-Beta-24h-150°C-rotation-M_2, Na-Beta-12 h-175°C-rotation-M_2, Na-Beta-17 h-175°C-rotation M_2, and Na-Beta-17 h-175°C-rotation-M_2, Na-Beta-24h-175°C-M_2 and Na-Beta-17h-150°C-M_2-GR-2h and Na-Beta-17h-150°C-rotation-M_2-GR-4h Beta zeolites exhibited highly crystalline phase pure structures. The physico-chemical characterization results of the synthesized Beta zeolites confirmed that the crystal structure, surface area, pore volume and pore size varied depending on the synthesis conditions. The largest average crystallite size (344 nm) using scanning electron microscopy was obtained for Na-Beta-24 h-175°C-rotation-M_2 and the second largest (340 nm) was achieved for Na-beta-12h-175°C-rotation-M_2, clearly indicating the influence of high temperature (175 °C) in the formation of Beta zeolite crystals.

Synthesized materials, prepared at 150 °C, were analyzed by Al-NMR. ^{29}Si and ^{27}Al both show almost identical spectra for all samples except the spectra for H-Beta-12h-static-150°C-M_2. It was inferred that 12 h of hydrothermal synthesis was not enough to form tetrahedral Al in the structure of Beta zeolite. The measurement of the acidic properties of the Beta zeolite using FTIR showed the presence of Brønsted and Lewis acid sites. Moreover, the number of Brønsted acid sites in H-Beta-17h-rotation-150°C-M_2 was higher compared to H-Beta-25, H-Beta-150 and H-Beta-300 [52-53].

References

1 E.M. Flanigen, R.W. Broach, S.T. Wilson in: S. Kulprathipanja (Ed.), Zeolites in industrial separation and catalysis, *Wiley-VCH*, **(2010)**, 618.

2 M.E. Davis, R.F. Lobo, Zeolite and molecular-sieve synthesis, *Chem. Mater*., 4 (**1992**) 756–768.

3 M.E. Davis, New vistas in zeolite and molecular-sieve catalysis, *Acc. Chem. Res.*, 26 (**1993**) 111–115.

4 M.E. Davis, Zeolites from a materials chemistry perspective, *Chem. Mater.*, 26 (**2014**) 239–245.

5 A. Corma, Inorganic solid acids and their use in acid-catalyzed hydrocarbon reactions, *Chem. Rev.*, 95 (**1995)** 559–614.

6 C.S. Cundy, P.A. Cox, The hydrothermal synthesis of zeolites: history and development from the earliest days to the present time, *Chem. Rev.*, 103 (**2003**) 663–701.

7 E. M. Flanigen, Chapter 2. Zeolites and molecular sieves: An historical perspective, *Stud. Surf. Sci. Catal.*, 137 (**2001**) 11 – 35.

8 D. P. Serrano, J. Aguado, J. M. Escola, J. M. Rodríguez, Influence of nanocrystalline hzsm-5 external surface on the catalytic cracking of polyolefins, *J. Anal. Appl. Pyrolysis.*, 74 (**2005**) 353–360.

9 D. P. Serrano, J. M. Escola, P. Pizarro, Synthesis strategies in the search for hierarchical zeolites, *Chem. Soc. Rev.*, 42 **(2013**) 4004 – 4035.

10 J. Pérez-Ramírez, C. H. Christensen, K. Egeblad, C. H. Christensen, J. C. Groen, Hierarchical zeolites: enhanced utilisation of microporous crystals in catalysis by advances in materials design, *Chem. Soc. Rev.*, 37 (**2008**) 2530 – 2542.

11 K. Egeblad, C. H. Christensen, M. Kustova, C. H. Christensen, Templating mesoporous zeolites, *Chem. Mater.*, 20 (**2008**) 946 – 960.

12 C. H. Christensen, K. Johannsen, E. Törnqvist, I. Schmidt, H. Topsøe, C. H. Christensen, Mesoporous zeolite single crystal catalysts: Diffusion and catalysis in hierarchical zeolites, *Catal. Today*, 128 (**2007**) 117 – 122.

13 D. H. Park, S. S. Kim, H. Wang, T. J. Pinnavaia, M. C. Papapetrou, A. A. Lappas, K. S. Triantafyllidis, Selective petroleum refining over a zeolite catalyst with small intracrystal mesopores, *Angew. Chem. Int. Ed.*, 48 (**2009**) 7645 – 7648.

14 Y. Sun, R. Prins, Hydrodesulfurization of 4,6-dimethyldibenzothiophene over noble metals supported on mesoporous zeolites, *Angew. Chem. Int. Ed.*, 47 (**2008**) 8478 – 8481.

15 C. H. Christensen, I. Schmidt, A. Carlsson, K. Johannsen, K. Herbst, Crystals in crystals – nanocrystals within mesoporous zeolite single crystals, *J. Am. Chem. Soc.*, 127 (**2005**) 8098 – 8102.

16 J. M. Escola, J. Aguado, D. P. Serrano, A. García, A. Peral, L. Briones, R. Calvo, E. Fernández, Catalytic hydroreforming of the polyethylene thermal cracking oil over Ni supported hierarchical zeolites and mesostructured aluminosilicates, *Appl. Catal.*, B 106 (**2011**) 405 – 415.

17 R. Srivastava, M. Choi, R. Ryoo, Mesoporous materials with zeolite framework: remarkable effect of the hierarchical structure for retardation of catalyst deactivation, *Chem. Commun.*, (**2006**) 4489 – 4491.

18 J. Kim, M. Choi, R. Ryoo, Effect of mesoporosity against the deactivation of MFI zeolite catalyst during the methanol-to-hydrocarbon conversion process, *J. Catal.*, 269 (**2010**) 219 – 228.

19 W. M. Meier, D. H. Olson, C. Baerlocher, Atlas of zeolite structure types, *Zeolites-Int. J. of Molec. Sieves*, **1996**, 405.

20 M.A. Camblor, J. Pérez-Pariente, Crystallization of zeolite Beta – effect of Na and K-ions, *Zeolites*, 11 (**1991**) 202 – 210.

21 K. Zhang, S. Fernandez, J. T. O'Brien, T. Pilyugina, S. Kobaslija, M. L. Ostraat,. Organotemplate-free synthesis of hierarchical beta zeolites. *Catal. Today*, 316 (**2017**), 26–30.

22 L.R.M. dos Santos, M.A.P. da Silva, S.C. de Menezes, L.S. Chinelatto, Jr., Y.L. Lam, Creation of mesopores and structural re-organization in Beta zeolite during alkaline treatment, *Microp. Mesopor. Mater.*, 226 (**2016**), 260-266.

23 K. Zhang, S. Fernandez, J. T. O'Brien, T. Pilyugina, S. Kobaslija, M. L. Ostraat, Organotemplate-free synthesis of hierarchical beta zeolites. *Catal. Today*, 234 (**2017**), 347–360.

24 G. Huang, P. Ji, H. Xu, J.-G. Jiang, L. Chen, P. Wu, Fast synthesis of hierarchical Beta zeolites with uniform nanocrystals from layered silicate precursor, *Microp. Mesopor. Mater.*, 248 (**2017**), 30-39.

25 M. Rutkowska, Z. Piwowarska, E. Micek, L. Chmielarz, Hierarchical Fe-, Cu- and Co-Beta zeolites obtained by mesotemplate-free method. Part I: Synthesis and catalytic activity in N_2O decomposition, *Microp. Mesopor. Mater.*, 209 (**2015**) 54–65.

26 Y. Jin, L. Zhang, J. Liu, S. Zhang, S. Sun, S. Asaoka, K. Fujimoto, Mesopore modification of beta zeolites by sequential alkali and acid treatments: Composition-dependent T-atoms removal behavior back donating to hierarchical structure and catalytic activity in benzene alkylation. *Microp. Mesopor. Mater.*, 248 (**2017**) 7–17.

27 Y. Fang, Y. Hu, X. Liang, S. Wang, S. Zuo, X. Gao, Z. Zhang, Microwave hydrothermal synthesis and performance of NaA zeolite monolithic adsorbent with honeycomb ceramic matrix. *Microp. Mesopor. Mater.*, 259 (**2018**) 116–122.

28 U. Khalil, O. Muraza, Microwave-assisted hydrothermal synthesis of mordenite zeolite: Optimization of synthesis parameters. *Microp. Mesopor. Mater.*, 232 (**2016**) 211–217.

29 R. A. García-Muñoz, D. P. Serrano, G. Vicente, M. Linares, D. Vitvarova, J. Čejka, Remarkable catalytic properties of hierarchical zeolite-Beta in epoxide rearrangement reactions, *Catal. Today*, 243 (**2015**) 141–152.

30 M. A. Camblor, A. Corma, A. Mifsud, J. Pérez-Pariente, S. Valencia, Synthesis of nanocrystalline zeolite beta in the absence of alkali metal cations. *Stud. Surf. Sci. Catal.*, 105 (**1997**) 341–348.

31 J. Aguado, D. P. Serrano, J. M. Rodrígueza, J. Aguado, Zeolite Beta with hierarchical porosity prepared from organofunctionalized seeds. *Microp. Mesopor. Mater.*, 115(3) (**2008**) 504–513.

32 V. Pashkova, V. Tokarova, L. Brabec, J. Dedecek, Self-templating synthesis of hollow spheres of zeolite ZSM-5 from spray-dried aluminosilicate precursor. *Microp. Mesopor. Mater.*, 228 (**2016**) 59–63.

33 J.M. Escola, D.P. Serrano, R. Sanz, R.A. Garcia, A. Peral, I. Moreno, M. Linares, Synthesis of hierarchical Beta zeolite with uniform mesopores: effect on its catalytic activity for veratrole acylation, *Catal. Today*, 304 (**2018**) 89-96.

34 A. R. do Nascimento, G. P. de Figueredo, E. M. F. Silva, M. A. F. Melo, D. M. A. Melo, M. J. B. de Souza, Synthesis, optimization and characterization of zeolite Beta (BEA): Production of ZSM-5 and $NaAlSiO_4$ as secondary phases, *Rev. Virtual Quim*, 9 (**2017**) 1570-1582.

35 F. Taborda, T. Willhammar, Z. Wang, C. Montes, X. Zou, Synthesis and characterization of pure silica zeolite beta obtained by an aging–drying method, *Microp. Mesopor. Mater.*, 143 **(2011)** 196–205.

36 N. P. William. van der Graaff, Guanna Li, B. Mezari, E. A. Pidko, E. J. M. Hensen, Synthesis of Sn-Beta with exclusive and high framework Sn content, *ChemCatChem*, 7 (**2015**) 1152-1160.

37 J. M. Escola, D. P. Serrano, R. Sanz, R. A. Garcia, A. Peral, I. Moreno, M. Linares, Synthesis of hierarchical Beta zeolite with uniform mesopores: effect on its catalytic activity for veratrole acylation, *Catal. Today*, 304 (**2018**) 89-96.

38 J. Jin, X. Ye, Y.Li, Y. Wang, L. Li, J. Gu, W. Zhaoa, J.Shi, Synthesis of mesoporous Beta and Sn-Beta zeolites and their catalytic performances, *Dalton Trans.*, 43 (**2014**) 8196-8204.

39 C. Manrique, A. Guzman, J. Pérez-Pariente, C. Márquez-Álvarez, A. Echavarría, Effect of synthesis conditions on zeolite Beta properties and its performance in vacuum gas oil hydrocracking activity, *Microp. Mesopor. Mater.*, 234 (**2016**) 347-360.

40 K. Möller, B. Yilmaz, R. M. Jacubinas, U. Müller, T. Bein, One-step synthesis of hierarchical zeolite Beta via network formation of uniform nanocrystals, *JACS*, 133 (**2011**) 5284-5295.

41 C. Bian, C. Zhang, S. Pan, F. Chen, W. Zhang, X. Meng, S. Maurer, D. Dai, A. Parvulescu, U. Müller, F. Xiao Generalized high-temperature synthesis of zeolite catalysts with unpredictably high space-time yields (STYs), J. Mater. Chem. *A*, 5 (**2017**) 2613-2618.

42 Z. Zhu, H. Xu, J. Jiang, H. Wu, P. Wu, Hydrophobic nanosized all-silica Beta zeolite: Efficient synthesis and adsorption application, *ACS Appl. Mater. Interfaces*, 9 (**2017**) 27273-27283

43 Powder Diffraction File 2 (PDF-2), sets 1-46, 1996 release, International Centre for Diffraction Data (ICDD).

44 Database of Zeolite Structures, http://www.iza-structure.org/databases/ [Cited 25.07.18].

45 Inorganic Crystal Structure Database (ICSD), version 3.7.0, http://www2.fiz-karlsruhe.de/icsd_home.html, [Cited 17.05.18]., Fiz Karlsruhe.

46 J. M. Newsam, M. M. J. Treacy, W. T. Koetsier, C. B. de Gruyter, Structural characterization of zeolite beta, *Proc. R. Soc. Lond. A*, 420 (**1988**) 375-405.

47 C.A. Emeis, Determination of integrated molar extinction coefficients for infrared absorption bands of pyridine adsorbed on solid acid catalysts, *J. Catal.*, 141 (**1993**), 347-354.

48 C. A. Fyfe, H. Strobl, G. T. Kokotailo, C. T. Pasztor, G. E. Barlow, S. Bradly, Correlations between lattice structures of zeolites and their ^{29}Si MAS n.m.r. spectra: zeolites KZ-2, ZSM-12, and Beta, *Zeolites*, 8(2) (**1988**) 132-136.

49 G. Engelhardt, D. Michel, High-resolution solid-state NMR of silicates and zeolites, *John Wiley & Sons*, **1987**, 485.

50 Z. Zhao, S. Xu, M. Y. Hu, X. Bao, C. H. F. Peden, J. Hu, Investigation of aluminum site changes of dehydrated zeolite H-Beta during rehydration process by high field solid state NMR. *J. Phys. Chem.*, 119 (**2015**) 1410-1417.

51 J. A. von Bokhoven, D. C. Konigsberger, P. Kunkeler, H. van Bekkum, A. P. M. Kentgens. Stepwise dealumination of zeolite Beta at specified T-sites observed with 27Al MAS and 27Al MQ MAS NMR. *J. Am. Chem. Soc.*, 122 (**2000**) 12842-12847.

52 A. Aho, N. Kumar, K. Eränen, T. Salmi, M. Hupa, D. Y. Murzin, Catalytic pyrolysis of biomass in afluidized bed reactor: Influence of the acidity of H-beta zeolite. *Proc. Saf. Environ. Prot.*, 85 (**2007**) 473–480.

53 A. Torozova, P. Mäki-Arvela, A. Aho, N. Kumar, A. Smeds, M. Peurla, R. Sjöholm, L. Heinmaa, D. V. Korchagina, K. P. Volcho, Heterogeneous catalysis for transformation of biomass derived compoundsbeyond fuels: Synthesis of monoterpenoid dioxinols with analgesic activity. *J. Mol. Catal. A. Chem.*, 397 (**2015**) 48–55.